JCI The Journal of Clinical Investigation

Angiopoietin-like protein 2 mediates vasculopathy driven fibrogenesis in a mouse model of systemic sclerosis

Dyuti Saha, … , Praveen K. Vemula, Colin Jamora

J Clin Invest. 2025. https://doi.org/10.1172/JCI177123.

Research In-Press Preview Cell biology Dermatology Vascular biology

Graphical abstract

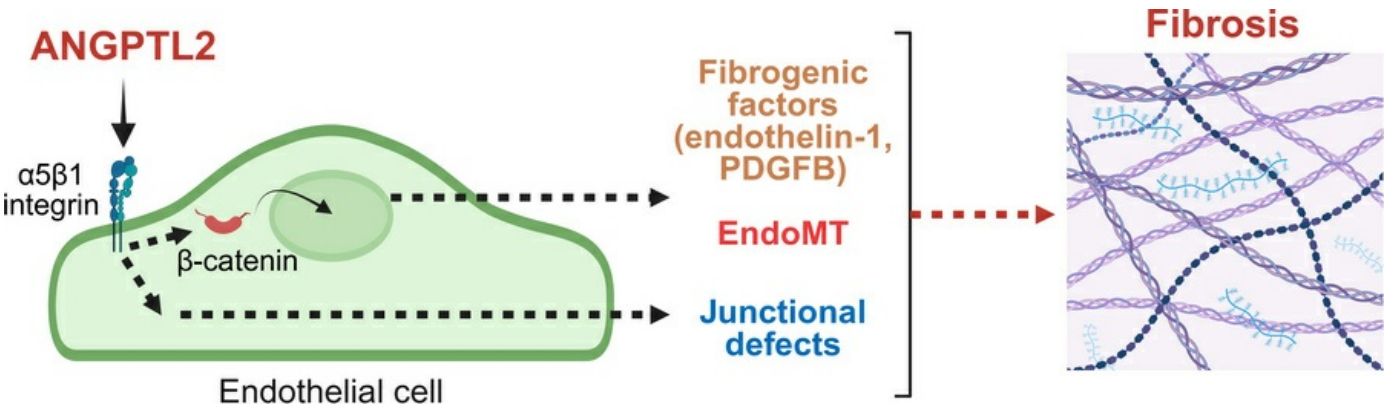

Angiopoietin-like protein 2 mediates vasculopathy driven fibrogenesis in a mouse model of systemic sclerosis

Dyuti Saha[1,2,3], Ravi Kiran Annadorai[1], Sujaya Thannimangalath[1], Neha Pincha[1], Sunny Kataria[1,3], Binita Dam[1,2], Abhik Dutta[1,4], Akshay Hegde[1,4], Ankita Hiwale[5], Venkatesh Ravula[5], Shagnik Saha[6], Lekshmi Minikumari Rahulan[7], Neha Nigam[8], Neha Singh[7], Vikas Agarwal[7], Praveen K. Vemula[5], Colin Jamora[1,3*]

1 IFOM-inStem Joint Research Laboratory, Institute for Stem Cell Science and Regenerative Medicine, Bangalore, India

2 Department of Biology, Manipal Academy of Higher Education, Manipal, India

3 Department of Life Sciences, Shiv Nadar Institution of Eminence, Delhi-NCR, India

4 School of Chemical and Biotechnology, Shanmugha Arts, Science, Technology and Research Academy, Thanjavur, Tamil Nadu, India

5 Laboratory of Chemical Biology and Translational Research, Institute for Stem Cell Science and Regenerative Medicine (DBT-inStem), Bangalore, India

6 Center of Excellence in Epigenetics, Department of Life Sciences, Shiv Nadar Institution of Eminence, Delhi-NCR, India

7 Department of Clinical Immunology and Rheumatology, Sanjay Gandhi Postgraduate Institute of Medical Sciences, Lucknow, India

8 Department of Pathology, Sanjay Gandhi Postgraduate Institute of Medical Sciences, Lucknow, India

*Corresponding author: Colin Jamora

Shiv Nadar Institution of Eminence

NH91, Tehsil Dadri, Greater Noida, Uttar Pradesh – 201314, India

Phone: 7011115898

Email: colin.jamora@snu.edu.in

Keywords: fibrosis, systemic sclerosis, vasculopathy, angiopoietin-like protein 2, claudin, tight junctions, endothelial cells, skin

The authors have declared that no conflict of interest exists

ABSTRACT

Vasculopathy is a common hallmark of various fibrotic disorders including systemic sclerosis (SSc), yet its underlying etiology and contribution to fibrogenesis remain ill-defined. In SSc the vasculopathy typically precedes the onset of fibrosis and we observed that this phenomenon is recapitulated in the *Snail* transgenic mouse model of SSc. The vascular anomalies manifest as deformed vessels, endothelial cell dysfunction and vascular leakage. Our investigation into the underlying mechanism of this phenotype revealed that angiopoietin-like protein 2 (ANGPTL2), secreted by the *Snail* transgenic keratinocytes, is a principal driver of fibrotic vasculopathy. In endothelial cells, ANGPTL2 upregulates pro-fibrotic genes, downregulates various junctional proteins, and prompts the acquisition of mesenchymal characteristics. Inhibiting endothelial cell junctional instability and consequently vascular leakage with a synthetic analog of the microbial metabolite Urolithin A (UAS03) effectively mitigated the vasculopathy and inhibited fibrogenesis. Thus, ANGPTL2 emerges as a promising early biomarker of the disease and inhibiting the vasculopathy inducing effects of this protein with agents such as UAS03 presents an appealing therapeutic avenue to reduce disease severity. These insights hold the potential to revolutionize the approach to the treatment of fibrotic diseases by targeting the vascular defects.

INTRODUCTION

Fibrosis is a pathological condition wherein deposition of extracellular matrix (ECM) components by activated fibroblasts leads to tissue stiffness and loss of function. Fibrotic diseases lead to ~40% of deaths worldwide (1) however the lack of effective treatments emphasizes the need for a thorough molecular understanding of fibrogenesis. In this context, the role of soluble factors such as TGFβ (2) and immune cells and inflammation (3) has been extensively studied for their contribution towards fibrosis development. However, targeting these pathways in clinical trials(s) have had limited success (4), suggesting the existence of compensatory/overlapping signalling cascades that require elucidation to facilitate effective therapy development.

Fibrotic skin diseases range from localized fibrotic lesions on the skin (seen in localized scleroderma) to conditions with widespread involvement of multiple organs in systemic sclerosis (SSc) (5, 6). Like many other fibrotic tissues, a prominent hallmark of SSc are defects in blood vessels in the skin (7). Interestingly, patient data reports that these vasculopathies manifest quite early in the disease progression (8) suggesting their potential role in promoting fibrogenesis. Examination of patient samples from SSc has revealed that the disease is marked by early endothelial damage, followed by the accumulation of immune cell infiltrates near the affected vasculature and eventually foci of ECM deposits by activated fibroblasts (9, 10). The early manifestation of vascular defects in the course of fibrogenesis suggests that pathways and factors involved in mediating vascular abnormalities could potentially be used both as early biomarkers of the disease as well as therapeutic targets.

While there have been a few mouse models developed to understand the mechanistic basis of SSc progression, most do not recapitulate all the facets of the disease condition (11, 12). For example, the genetic mouse model of SSc, *Tsk2/+* exhibits dermal fibrosis and inflammation but shows an absence of vascular defects (13, 14), whereas the *Tsk1/+* mouse exhibits abnormal vascular tone but lacks a robust inflammatory response (15, 16). On the other hand, chemically-induced models such as the Bleomycin induced fibrotic model (17, 18) faithfully recapitulate the dermal fibrosis and inflammation associated with SSc while only partially recapitulating the vasculature defects. Therefore, there was a need for a mouse model system that recapitulates a larger spectrum of SSc characteristics in order to elucidate the molecular mechanism of SSc vasculopathy.

We have previously developed a transgenic (tg) mouse model mimicking SSc skin by ectopically expressing the transcription factor Snail in the basal layer of keratinocytes of the mouse skin. Snail has been reported to be upregulated in various fibrotic conditions (19–22) including SSc (23). The *Snail* tg mouse skin recapitulates various histological and molecular features of SSc such as the increased dermal thickness, ECM deposition and increased inflammation. Similar to the progression of SSc, the fibrosis in the *Snail* tg mouse is long-lasting and originates in the skin and progresses to the involvement of internal organs (23). Although defects related to the blood vessels such as Raynaud's phenomenon was observed in the *Snail* tg skin (23), it remains to be determined to what extent the *Snail* tg skin recapitulates SSc vasculopathy. The presence of SSc-like vascular defects in the *Snail* tg skin would position this mouse model as a platform to elucidate the underlying mechanisms of SSc vasculopathy and the contribution of vascular defects to fibrogenesis.

RESULTS

SSc-associated vasculopathy is recapitulated in the adult *Snail* transgenic skin

We have previously reported that the *Snail* tg mouse recapitulates many of the diagnostic features of SSc (23–25). We thus investigated whether the *Snail* tg mouse skin could recapitulate the various aspects of vasculopathy associated with SSc. We undertook a morphometric analysis of the cutaneous vasculopathy in 2-month-old adult *Snail* tg mice with the markers used to profile for human (26) and mouse (18, 27) fibrotic skin. Staining of the back-skin of adult *Snail* tg mouse with the endothelial cell marker PECAM1 (platelet endothelial cell adhesion molecule 1) revealed that *Snail* tg skin vessels had increased morphological distortions in the form of altered vascular structures compared to its wild type counterpart (Figure 1A). Upon performing morphometric analysis, we observed a significant increase in vascular density (Figure 1B) and percentage of mean vessel area (Figure 1C) in the *Snail* tg skin compared to the wild type skin. Distorted vasculature is often an early driver of pathological neovascularization with hyperproliferation of endothelial cells (28). Consistent with this, we observed a two-fold increase in the total number of endothelial cells and ~ 9-fold increase in the number of Ki67 positive endothelial cells in the *Snail* tg skin vasculature compared to wild type skin (Figure 1, D-F).

We next analysed gene expression changes related to SSc vasculopathy. Endothelin1(*Edn1*), a marker of endothelial cell damage and dysfunction found in SSc skin (29, 30) is increased in the *Snail* tg skin (Figure 1G). Another important factor that is upregulated in SSc patients is platelet-derived growth factor B (PDGFB) that is constitutively secreted from endothelial cells and affects both perivascular cells as well as activate surrounding fibroblasts (31). Pdgfb is likewise upregulated in the whole

skin and isolated dermal endothelial cells of *Snail* tg mouse compared to wildtype (Figure 1H).

To investigate whether the blood vessels in *Snail* tg skin are functionally compromised, we examined the vascular integrity with the Evan's blue dye leakage assay. We observed that the *Snail* tg skin had increased blue color indicating vascular leakage. Upon quantification, we found that *Snail* tg skin had a nearly three-fold increased dye extravasation into tissue from the vasculature indicating the perturbation of vessel integrity (Figure 1I). We hypothesized that disruption of endothelial cell-cell adhesion underlies the increased vascular permeability in the *Snail* tg skin and analysed the status of the tight junction protein claudin5. In the *Snail* tg skin, the vessels exhibited a reduction in claudin5 levels (Figure 1J) and upon quantification we observed a significant decrease in PECAM1 and claudin5 double positive vascular structures (Supplementary Figure 1A). Similarly, upon analysis of the adhesion junction protein VE-Cadherin (vascular endothelial cadherin), PECAM1 and VE-Cadherin double positive vascular structures were also significantly reduced in the *Snail* tg skin (Figure 1K, Supplementary Figure 1B). In line with this, we found that isolated endothelial cells from the *Snail* tg skin exhibited a decrease in gene expression of various junction proteins such as claudin5 (*Cldn5*), VE-Cadherin (*Cdh5*), ZO1 (*Tjp1*), occludin (*Ocln*) and JAM3 (*Jam3*) (Supplementary Figure 1C).The loss of endothelial barrier stability has been hypothesized to prime endothelial cells to adopt a mesenchymal phenotype (32, 33). A partial or complete acquisition of mesenchymal characteristics can cause endothelial cells to adopt features of myofibroblasts in SSc skin (28, 34). We observed upregulated mRNA expression of myofibroblast genes *Ctgf* (connective tissue growth factor) and *Acta2* (α-smooth muscle actin) in isolated endothelial cells from the *Snail* tg skin (Figure 1L). Also, the *Snail* tg skin exhibited a significant increase in

αSMA/PECAM1 double positive vessels when compared to wildtype skin (Figure 1M, Supplementary Figure 1D).

Overall, the *Snail* tg skin reproduces key vascular abnormalities observed in SSc, providing a valuable platform to profile the developmental progression of the vasculopathy and its molecular underpinnings.

Developmental analysis of *Snail* tg skin reveals that vasculopathy defects occur early in fibrogenesis

Since vasculopathy is an early phenomenon in SSc disease progression (7), we hypothesized that it may have an active role in promoting fibrogenesis. To interrogate whether the *Snail* tg skin also exhibits early vasculopathy that precedes the thickening of the dermis, we performed a developmental analysis of the vasculopathy phenotype. Previously, we have observed increased dermal thickening (a readout for fibrosis) as early as postnatal day 9 in the *Snail* tg skin which increases progressively to adulthood (23). We therefore analysed the vascular defects via PECAM1 staining at postnatal (P) days 3, 7, and 9 and observed an increase in vessel density and percentage of mean vessel area as early as P3 in the *Snail* tg skin (Figure 2A, Supplementary Figure 2, A and B). Moreover, an increase in the overall number of endothelial cells as well as Ki67/PECAM1 double positive cells at P3 indicates the hyperproliferation of endothelial cells (Figure 2B, Supplementary Figure 2, C and D). Likewise, markers of endothelial damage such as *Edn1* (Figure 2C) and *Pdgfb* (Figure 2D) were upregulated initially from postnatal day 3 suggesting that signalling pathways mediating vascular defects are initiated early in disease development in the *Snail* tg skin. We further tested the vascular integrity at these stages by performing the Evan's blue dye leakage assay. As early as P3 the *Snail* tg skin exhibits increased vascular permeability (Figure 2E). In line with this, we detected disruptions in claudin5 starting at P3, where it appeared in a punctate pattern on the surface of certain vascular structures (Figure 2F). Additionally, the number of vascular structures co-expressing claudin5 and PECAM1 significantly decreased (Supplementary Figure 2E). Moreover, some αSMA/PECAM1 double-positive vessels were first observed at P3 and became more prominent in the P7 *Snail* tg skin (Figure 2G and Supplementary Figure 2F).

Notably, this suggests that endoMT (endothelial-mesenchymal transition)-related changes in these vessels are linked to junctional destabilization.

Overall, our findings suggest that vasculopathy emerges in the *Snail* tg skin before marked dermal thickening develops, mirroring the early vascular defects seen in SSc patient skin.

Angiopoietin-like 2 (ANGPTL2) secreted by *Snail* tg keratinocytes is necessary to induce dermal vasculopathy

Previously we reported that extracellular factors such as Mindin (23) and PAI1 (24) are secreted from *Snail* tg keratinocytes and elicit fibrotic responses by activating dermal fibroblasts. We thus investigated whether the secretome of *Snail* tg keratinocytes can elicit the vascular defects found in the transgenic mouse. Conditioned media from *Snail* tg keratinocytes was able to induce vascular thickening and increased density in wild type skin explants that recapitulated the vasculopathy found in the transgenic skin (Supplementary Figure 3, A and B). The next question was the identity of the vasculopathy inducing factor(s) in the secretome of the *Snail* tg keratinocytes. Though Mindin or PAI1 play critical roles in the fibrogenesis in the *Snail* tg skin, they are not required for the vasculopathy (Supplementary Figure 3, C-F). Another factor that is highly expressed (Figure 3A) and secreted (Figure 3, B and C) primarily from the epidermal keratinocytes of the *Snail* tg skin at P3 is Angiopoietin-like 2 (ANGPTL2) (Supplementary Figure 4A). Bioinformatic analysis of *Angptl2* gene expression in published datasets of keloid (35) and SSc (36) patients and fibrotic diseases of other human organs such as the lung (37), kidney (38) and liver (39) revealed that *Angptl2* is upregulated in the diseased skin compared to healthy skin controls (Figure 3D, Supplementary Figure 4, B-D). In addition, ANGPTL2 has been reported to be involved in pathological angiogenesis in diseases such as cancer (40). Therefore, we hypothesized that ANGPTL2 might also play a role in fibrotic vasculopathy in SSc skin. We found that ANGPTL2 is secreted from SSc patient skin suggesting a possible contribution in disease manifestation (Figure 3E).

To test the role of ANGPTL2 in SSc vasculopathy, we generated a *Angptl2* KO mouse in the *Snail* tg background (Supplementary Figure 4E). We first assessed whether the

presence of ANGPTL2 was required for vasculopathy-related characteristics in cultured endothelial cells. Conditioned media containing secreted proteins from *Snail* tg keratinocytes upregulated vasculopathy related genes such as *Edn1* and *Pdfgb*, while promoting an endoMT phenotype as assessed by a collagen contraction assay. Notably, these vasculopathy-related effects were abrogated when using conditioned media from *Snail* tg*/Angptl2* KO keratinocytes (Figure 3, F and G).

Further, we assessed the necessity of ANGPTL2 in vasculopathy and fibrogenesis in the *Snail* tg adult mouse in vivo. We found that the vascular density (Figure 4, A-C) and vascular permeability (Figure 4D) in the *Snail* tg*/Angptl2* KO mouse was restored to wild type levels. Furthermore, the increased Collagen I levels (Figure 4, E and F) and dermal thickness (Figure 4, G and H) (readout of fibrosis) in the *Snail* tg skin was significantly reduced in the absence of ANGPTL2. Overall, this data indicates that ANGPTL2 is an important factor that drives the vasculopathy and fibrotic phenotypes in the *Snail* tg skin.

ANGPTL2 **is sufficient to drive various features of dermal vasculopathy**

We investigated the extent to which ANGPTL2 is sufficient to drive the vasculopathy observed in the skin of the *Snail* tg mouse. Using an ex-vivo explant assay, we found that ANGPTL2 can promote the dilation and swelling of vessels (Figure 5A), which recapitulates the changes in the vasculature in the *Snail* tg skin. ANGPTL2 also caused significant upregulation in mRNA levels of factors involved in SSc vasculopathy such as *Edn1* (Figure 5B) and *Pdgfb* (Figure 5C) in skin explants and the mouse endothelial cell line SVEC4-10. In line with this, secreted factors from ANGPTL2 treated endothelial cells could drive upregulation of myofibroblast genes *Acta2* and *Ctgf* (Figure 5D) as well as induce increased contraction (Figure 5E) in dermal fibroblasts. However, ANGPTL2 did not have a direct effect on endothelial cell proliferation in vitro (Supplementary Figure 5, A and B).

Endothelial cells isolated from the *Snail* tg skin exhibited upregulation of myofibroblast markers, underlying our hypothesis that ANGPTL2 could play a role in promoting endoMT. Levels of myofibroblast markers (*Acta2*, *Ctgf*, *Fsp1* (Fibroblast specific protein 1), *SM22a* (transgelin) and *Cnn1* (calponin 1)) were upregulated in SVEC4-10 cells upon ANGPTL2 treatment (Figure 5F and Supplementary Figure 5, C and D). Further, ANGPTL2 mediated a change in actin distribution (Supplementary Figure 5E) which is consistent with endothelial cells undergoing endoMT(41, 42). These observations recapitulate colocalization of fibroblast and endothelial markers (43) found in human SSc. We further examined whether these changes in the characteristic of endothelial cells resulted in alterations in vasculature functions. ANGPTL2 imparted contractile behaviour in endothelial cells in collagen matrices (Figure 5G) and induced vascular leakage in a sheet of SVEC4-10 cells *in vitro* (Figure 5H).

Vascular dysfunction is often a consequence of perturbed tight junctions due to the loss of claudin5 expression (44). Consistent with this, qPCR analysis revealed that mRNA levels of the tight junction protein claudin5 was significantly downregulated in SVEC4-10 cells treated with ANGPTL2 (Figure 5I). Moreover, the distribution of claudin5 and another junctional protein (VE-Cadherin) was perturbed in treated endothelial cells (Supplementary Figure 5, F and G). Considering the important role of claudin5 in maintaining vascular integrity (44, 45), we further tested if the acquisition of mesenchymal behaviours was likewise dependent on claudin5. To counteract the ANGPTL2 mediated loss of claudin5, a stable SVEC4-10 cell line with constitutive claudin5 overexpression (SVEC 4-10-C5) was generated. SVEC 4-10-C5 cells were refractory to increased contractility in collagen matrices upon ANGPTL2 treatment when compared to the parental SVEC 4-10 cells (Figure 5J).

We then investigated the signalling pathway activated by ANGPTL2 in endothelial cells. The integrin α5β1 has been reported as a receptor for ANGPTL2 in other contexts (46) therefore we tested if ANGPTL2's effect in our system was dependent on this receptor. We found that blocking integrin α5β1 using a specific inhibitor (ATN-161) abrogates the effects of ANGPTL2 (Figure 6, A and B). Interestingly, previous reports had indicated that β-catenin (a signalling component closely associated with integrin α5β1 and junctional proteins) has roles in mediating endoMT (47). Interestingly, endothelial cells treated with ANGPTL2 exhibit a change in β-catenin localization (Figure 6C). Inhibiting β-catenin using XAV-939 inhibitor blocked the increased gene expression of *Edn1* and *Pdgfb* (pro-fibrotic factors) as well as *Acta2* and *Ctgf* (markers of activated fibroblasts) (Figure 6D). Moreover, inhibition of β-catenin abrogated the ANGPTL2 induced increase in the contractile behavior of the cells (Figure 6E). Altogether these data reveal β-catenin's crucial role as a

downstream mediator of ANGPTL2's effect on the endoMT and the production of pro-fibrotic factors.

ANGPTL2 mediated vasculopathy is abrogated by UAS03

We investigated whether upregulation of tight junction proteins such as claudin5 through chemical modalities would be an effective mechanism to inhibit the ANGPTL2 driven vasculopathy. We used a synthetic analog of a gut metabolite Urolithin A (UAS03), which was previously shown to restore the disrupted epithelial barrier by upregulating tight junction proteins in a mouse model of inflammatory bowel disease (48). We tested whether this function is conserved for endothelial cell junctions andfound that UAS03 treatment counteracts the decrease of claudin5 mRNA induced by ANGPTL2 in SVEC 4-10 cells (Figure 7A). In line with this effect on gene expression, UAS03 could also block the ANGPTL2-induced vascular leakage through an endothelial sheet in vitro (Figure 7B). We further interrogated if UAS03 could counteract the other vasculopathy defects mediated by ANGPTL2. Increased mRNA levels of *Edn1* (Figure 7C) and *Pdgfb* (Figure 7D) induced by ANGPTL2 treatment were restored to control levels in the presence of UAS03. We also observed that UAS03 treatment decreased mRNA levels of the endoMT markers *Acta2*, *Ctgf* and *Fsp1* induced by ANGPTL2 (Figure 7E). Consistent with the gene expression changes, UAS03 also blocked ANGPTL2 mediated increased contractility of endothelial cells in collagen matrices (Figure 7F). In sum, our data reveals that utilization of UAS03 is an effective method for mitigating the vasculopathy induced by ANGPTL2 in vitro.

We next interrogated whether UAS03 is effective in reducing the fibrotic phenotype in vivo. Intraperitoneal injections of UAS03 in mice from neonates (P3) to adulthood (P60) reduced the vascular leakage in the adult *Snail* tg animals to wild type levels (Figure 7G). Moreover, both vascular density and mean vessel area were significantly reduced upon injection of UAS03 in the *Snail* tg skin (Figure 7H, Supplementary Figure 6, A and B). We tested if the protective effects of UAS03 on the vasculature likewise

impacts fibrogenesis in the *Snail* tg mice. We observed a significant decrease in dermal thickness (Figure 7I) and Collagen I protein levels (Figure 7J) in UAS03 injected *Snail* tg mice compared to vehicle control at P60.

Inflammation is a hallmark of fibrosis and is facilitated by the recruitment of immune cells into the tissue through leaky vessels. Among these immune cells, macrophages are well-known to be increased in many fibrotic conditions. We observed that the ~4-fold increase of $CD11b^+$ cells (macrophages) in the *Snail* tg skin was substantially decreased in UAS03 injected tg mice (Figure 7K). We thus assessed if the UAS03-mediated decrease in the dermal fibrosis in the Snail tg skin is secondary to its effect on macrophage reduction. Interestingly, depletion of macrophage number with the chemical clodronate (Supplementary Figure 7, A and B) was not sufficient to reduce the increased dermal thickness (Supplementary Figure 7C) and Collagen I protein levels (Supplementary Figure 7, D and E) in the *Snail* tg mice skin compared to vehicle control.

UAS03 enhances tight junction while inhibiting pro-angiogenic/fibrogenic gene expression

To examine the mechanism of action of UAS03 on the vasculature in the *Snail* tg skin, we performed RNA seq analysis of SVEC 4-10 endothelial cell line treated with this synthetic metabolite. Based on adjusted p-value (q-value) of 0.05, 7554 genes were differentially expressed (Supplementary Table 1). Furthermore, based on the fold change cut-off of 1.5, 1658 genes were significantly upregulated and 2093 genes significantly downregulated (Figure 8A and B). Among the top genes based on significance and fold change, genes such as *Angptl7* and *Fxyd3*, which are implicated in pro-angiogenic effects, were downregulated upon treatment with UAS03 (49, 50). On the other hand, among the top upregulated genes was *Cyp2c55* which has been reported to have roles in physiological functions in endothelial cells such as maintenance of vascular tone (51). This unbiased approach suggests that UAS03 has an overall role in maintaining the homeostatic state of endothelial cells.

Given the previous report from the Vemula group (48) and our data (Figure 7A) we focused on the expression of endothelial junction proteins in the RNA Seq data. In addition to*Cldn5*, *Cldn25* was upregulated in UAS03 treated cells (Figure 8B). Furthermore, the expression of the junction protein *Pecam1*, which has been previously reported to promote the barrier integrity of endothelial cells (52), was also upregulated in UAS03 treated cells. In addition, we also observed upregulation of the tight junction protein *Tjp1* by UAS03 in the dataset however it was below the 1.5-fold cut-off used for our analysis (absolute fold change: 1.26). Interestingly, the adhesion junction protein VE-Cadherin (*Cdh5*) did not exhibit a statistically significant change in the RNA seq dataset but we observed an increased expression through qPCR analysis (Supplementary Figure 8). Altogether, these data indicate that UAS03

promotes endothelial junction stabilization through upregulation of junction components. This provides a mechanistic framework for the ability of UAS03 to inhibit vascular leakage in the *Snail* tg skin and thereby impede fibrogenesis (Figure 7).

GO term enrichment analysis using gProfiler2 (Supplementary Table 2) revealed an upregulation of genes involved in “response to stress”, and “DNA damage response” (Figure 8C). For instance, genes such as *Hmox1* and *Cyp1b1*, which have protective roles against oxidative damage, were among the upregulated genes (Figure 8B). This is consistent with reports of UAS03’s protective role against oxidative stress in gut epithelial cells (48) and suggests this function may likewise be conserved in endothelial cells.

Our data demonstrates that UAS03 treatment in endothelial cells and *Snail* tg mice reduced vasculopathy and fibrosis (Figure 7). In line with this, processes such as “angiogenesis”, “positive regulation of angiogenesis”, “endothelial cell proliferation”, “epithelial to mesenchymal transition”, and “mesenchyme development” were within the downregulated category (Figure 8D). This implies that UAS03 can provide a protective effect against ANGPTL2 by downregulating genes that would otherwise promote pathological angiogenesis and acquisition of mesenchymal phenotypes in endothelial cells. In addition, we found that terms such as “extracellular matrix structural constituents” and “collagen biosynthetic process” were also within the downregulated category. In line with this, various collagen genes such as *Col1a1* were downregulated by UAS03 (Figure 8B). This indicates that UAS03 supresses pro-fibrotic gene expression in endothelial cells, potentially contributing towards decreased fibrosis observed in treated *Snail* tg mice.

Our data suggests that various vasculopathy related gene expression changes mediated by ANGPTL2 are driven through β-catenin (Figure 6, C-E). Notably, terms

such as “Wnt signalling pathway” and “Wnt protein binding” were in the downregulated category, suggesting that UAS03 is capable of suppressing β-catenin signalling pathways that fuel fibrosis.

Altogether these observations support the notion that vascular defects have an important contribution to fibrogenesis in the *Snail* tg mouse. Moreover, these findings position the synthetic metabolite UAS03 as a potential therapeutic strategy against vasculopathy in fibrotic skin conditions such as SSc, and thereby substantially reduce tissue fibrosis.

DISCUSSION

Using a mouse model that recapitulates many of the clinical features of SSc (23), we have elucidated the mechanisms underlying vasculopathy that is a hallmark of this and many fibrotic diseases. Our work positions ANGPTL2 secreted from *Snail* tg keratinocytes as a major driver of the vasculopathy observed in the fibrotic skin. ANGPTL2 upregulates fibrogenic molecules in endothelial cells, downregulates canonical endothelial junction protein claudin5 and mediates acquisition of mesenchymal characteristics. The synthetic metabolite UAS03 counteracts the effects of ANGPTL2 in endothelial cells and reduces fibrosis in the *Snail* tg skin in part by reversing the downregulation of claudin5 (Figure 9). These observations are consistent with a previous report that the transgenic overexpression of *Angptl2* in the skin appears to partially phenocopy the *Snail* tg mouse, and in particular the vascular leakage (46).

Previous reports in SSc patient skin indicated that the vasculopathy occurs in progressive stages – “early” (marked by hyperangiogenesis, giant capillaries), “active” (marked by aberrant angiogenesis and morphological changes) and “late” (marked by loss of angiogenesis and avascular areas)(53). Our investigations of the status of the vasculature in the dorsal skin of the neonatal to adult (two-month-old) *Snail* tg mouse indicate that it represents the early to active stages of vasculopathy seen in SSc patient skin. Markers indicative of the fibroproliferative stage of SSc include proangiogenic factors such as vascular endothelial growth factor (VEGF) (54). Our previous work has demonstrated upregulation of VEGF in the *Snail* tg skin (55). Furthermore, Ki67 staining (Figure 1D) is consistent with proliferation driving higher vascular density (which has been quantified in Figure 1B). Cumulatively the evidence of the pro-angiogenic signalling further supports our claim that the *Snail* tg skin

represents the early stages of the disease at the time points investigated in this study. Although there is an observed increase in vascular density and numbers, the quality of the vasculature is compromised leading to leakage. This can be compared to cancer angiogenesis wherein there is formation of many new vessels but their quality is poor (56). The loss of vasculature (a feature of the late stage of the disease) might be observed much later in the lifetime of the *Snail* tg mouse which we have not included in this study. We have previously reported necrosis in the tail of the *Snail* tg mouse (23) and this could be representative of the loss of vessels. The majority of SSc patients seek medical treatment at later stages of the disease when destructive vasculopathy is observed. We believe that the early and active vasculopathy is faithfully recapitulated in the *Snail* tg skin in the ages we have included in the study and this would be a useful platform for identifying biomarkers for detecting early stages of the disease as well as developing therapeutics to combat the disease development before severe damage.

To date, it has not been clearly elucidated whether vasculopathy is a cause or a secondary effect of fibrosis in diseases such as SSc. Our work positions vasculopathy as an integral component driving fibrogenesis rather than a mere symptom of the disease. An outstanding question is how vasculopathy connects to other aspects of the disease pathology such as inflammation. Platelet activation has recently been hypothesized to be an important link between vasculopathy and inflammation in SSc (57). Platelets contain granules which store various factors that can be involved in SSc vasculopathy, which includes PDGF and VEGF (58). Intact vessel walls in unaffected vasculature usually prevents any stimuli causing platelet activation, however activated platelets can release granules containing these factors as well as molecules with pro-inflammatory activities. Endothelial dysfunction is an early event of SSc pathogenesis

which leads to platelet activation (57). Along with ANGPTL2-mediated junctional perturbation this can potentially be an early inducer of platelet activation setting in motion the subsequent changes in the pathogenesis of SSc.

An interesting observation in our study is that vascular defects and secretion of ANGPTL2 initiates in neonatal stages in the *Snail* tg skin. Previous reports have revealed that vasculopathy precedes other pathological features in SSc patient skin (59) and our data concurs with this clinical observation. This leads us to propose that ANGPTL2 can serve as a possible biomarker for detecting SSc like pathologies at an early stage before the manifestation of dermal thickening and accumulation of ECM, which are gross indications of fibrosis. Therapeutic modalities targeting ANGPTL2 can also potentially be of relevance in fibrotic diseases beyond SSc. Our analysis of published datasets has revealed upregulation of *Angptl2* in other fibrotic tissues such as the lung, kidney and liver (Supplementary Figure 4B). In addition to fibrosis, vascular dysfunction is an integral component in the development of several pathologies such as inflammatory diseases and cancers (60, 61) which likewise exhibit elevated levels of ANGPTL2 (62).

Together with previous reports, our data suggests that ANGPTL2 does not have a role in homeostasis. ANGPTL2 is not required for normal vascular development and the loss of ANGPTL2 in mice (46) or zebrafish (63) do not affect the animal's viability and fertility. Furthermore, we observed no prominent effect on wound closure in the *Angptl2* KO mouse skin (Supplementary Figure 9A). This suggests that the role of ANGPTL2 is primarily in pathological scenarios. Consistent with this, previous reports have shown ANGPTL2 to have important roles in tumor angiogenesis in various cancers (40, 64, 65). This indicates that a specific inhibitor to ANGPTL2 would likely have less side effects on normal tissue and thus have a high therapeutic potential.

As vasculopathy is a prominent feature of fibrotic diseases, previous therapies targeted factors such as Endothelin1 (66) and VEGF (67). Although promising in pre-clinical studies, they yielded limited success in clinical trials (66, 67). Therefore, it may be beneficial to target upstream mediators of these pathways that would theoretically have a broader effect on multiple downstream pathways. Our work has revealed that UAS03 targets multiple pathways downstream of ANGPTL2 leading to reduction in vasculopathy mediated fibrogenesis. The metabolite Urolithin A and its synthetic analog UAS03 have previously been reported to aid in gut epithelial junctional stability and in the reduction of inflammation in a mouse model of inflammatory bowel disease (48). Although previous reports attributed its anti-inflammatory effects to an inhibition of macrophage activity, blocking activated macrophages via clodronate liposomes in our study was not sufficient to reduce the vasculopathy and fibrosis in the *Snail* tg skin (Supplementary Figure 7). Therefore, utilizing UAS03 as a therapy would not only affect inflammation but other important signalling pathways that drive fibrogenesis. Interestingly, UAS03 treated animals did not exhibit a defect in wound closure suggesting its effect is limited to pathological scenarios (Supplementary Figure 9B). Therefore, our work provides important evidence supporting using UAS03 as a potential therapeutic approach for vasculopathy mediated fibrosis development.

METHODS

Sex as a biological variable

Mice of both sexes were used for the study and similar results were observed. Clinical samples from SSc patients were all from female donors.

Animal studies

WT (CD1) mice were obtained from The Jackson Laboratory. The K14-*Snail* tg mice was engineered as described previously (68). The *Angptl2* KO mouse was developed in the Mouse Genome Engineering Facility at Bangalore Life Sciences Cluster according to previous reports (46). The *Snail* tg/*Angptl2* KO mouse was developed by breeding K14-*Snail* tg and *Angptl2* KO mice. The *Snail* tg/*Mindin* KO mouse and *Snail* tg/*Pai1* KO mouse were developed as previously reported (23, 24).

Immunostaining and histology

Skin tissue was embedded in OCT (Leica) for sectioning. 20-30μm-thick sections, whole skin mounts or cells on coverslips were fixed using 4% paraformaldehyde and used for staining. Haematoxylin/Eosin staining was performed to observe tissue histology. The primary antibodies and dilutions used for immunofluorescence staining were: PECAM1 (BD, Cat No: 550274, 1:150), Ki67 (Abcam, Cat No: AB16667, 1:200), claudin5 (Invitrogen, Cat No: 34-1600, 1:50), VE-Cadherin (BD Biosciences, Cat No: BD550548, 1:50), Angptl2 (R&D, Cat No: AF1444, 1:50), αSMA (Sigma, Cat No: A2547, 1:200), Collagen I (Abcam, Cat No: AB21286, 1:200), β-catenin (Millipore, Cat No: 05-665, 1:500), CD11b (DSHB, Cat No: M1/70.15.11.5.2, 1:200). Alexa Fluor 488 and Alexa Fluor 561–labelled secondary antibodies (Jackson ImmunoResearch) were used at a dilution of 1:300. Alexa Fluor 568 Phalloidin (Invitrogen, Cat No: A12380) was used to stain actin. Nuclei were marked by DAPI.

Image collection and analysis

Imaging was performed with an Olympus IX73 microscope, FV3000 confocal microscope or Nikon A1R confocal microscope. Images were analysed on the Fiji (ImageJ) software. For morphometric analysis of blood vessels in the skin, vessel density was calculated by counting total vessel profiles divided by area of tissue in mm^2; Percentage mean vessel area was calculated as: (total vessel area/total tissue area) X 100. Collagen staining was quantified by integrated density measurement of the staining in the dermal region. Dermal thickness was quantified by measuring the area of the dermis in the H&E-stained sections. Quantifications for claudin5, VE-Cadherin and αSMA were done by counting double-positive vascular structures for PECAM1 and these markers respectively. 3 fields of interest (FOI) were analysed per biological replicate for quantification of images.

RNA extraction, cDNA synthesis and qRT-PCR

Total RNA was extracted from skin biopsies and cell lysates using RNAiso Plus Reagent (Takara, Cat No: 9109) according to the manufacturer's protocol. cDNA was prepared using PrimeScript cDNA synthesis kit (Takara, Cat No: 2680A) according to the manufacturer's instructions. Quantitative PCR (qPCR) was performed using PowerUp SYBR Green Master Mix (Applied Biosystems, Thermo Fisher Scientific, Cat No: A25742) with Bio-Rad CFX384 thermal cycler. TBP expression was used for normalization. The primers used are listed in Table 1.

Evan's Blue Dye Injection Assay

Evans Blue dye (1% w/v in PBS) (Sigma, E2129) was injected into the retro-orbital sinus of the mice according to body weight (60mg/kg). The mice were then euthanized and dorsal skin tissue was harvested. The tissue samples were air dried and then

incubated with formamide at 55°C to extract the Evan's blue dye into solution. The absorbance of this solution was measured at 620nm. Extravasated Evan's blue dye (ng per mg of tissue) was calculated using a standard curve.

FACS based isolation of cells from mouse skin

Dorsal skin of either P3 or adult (P60) wildtype and *Snail* tg mice were taken and all the hair removed. For P3 mice, the dermis was separated from the skin by incubating in 1 mg/ml dispase for 1 hour at 37 °C. For P60 mice the whole skin was processed. The tissue was digested with 2.5 mg/ml collagenase IV (Gibco) for either 45 mins or 2 hours respectively at 37°C. The cell suspensions were stained with PECAM1-FITC antibody (MACS Miltenyi Biotech, Cat No: 130-102-970, 1:50) or CD45-PE antibody (MACS Miltenyi Biotech, Cat No: 130-102-781, 1:100) at 4°C for 30 mins. $PECAM1^+$, $CD45^+$ and lineage negative cells were sorted from this cell suspension using BD-FACS Aria Fusion or ARIA III. Laser delay and area scaling were done using BD Sphero beads. ACD beads were used for setting drop delay. Unstained samples were used for setting the voltages. The cell population was gated using an SSC-A and FSC-A plot. A diagonal gate was made to select single cells using an FSC-A and FSC-H plot. The dead cell population was identified by staining with Propidium iodide (PI; Sigma P4864) and dead cell population < 15% of all events and < 10% of gated cells was considered for proceeding. Single-stained PECAM1 and CD45 samples were then recorded and color compensation performed. Thereafter, co-stained tubes of samples were used to sort $PECAM1^+$, $CD45^+$ and lineage negative cells. The sorted cells were pelleted at 100g and RNA extracted directly as described previously.

Cell culture and preparation of conditioned media

Mouse endothelial cell line SVEC4-10 (ATCC® CRL-2181™) was purchased from ATCC. SVEC4-10 cells were cultured in DMEM high-glucose media with 10% FBS. For all staining of SVEC 4-10 cells, cells were grown on a coverslip coated with 50µg/ml Collagen I solution till they formed an endothelial sheet and treatments done subsequently. A SVEC4-10 cell line with constitutive claudin5 overexpression (SVEC4-10-C5) was developed by transfecting pcDNA3.1 plasmid containing the mouse *Cldn5* gene.

Primary mouse keratinocytes were isolated from epidermis of P3 pups and either directly processed for RNA isolation or cultured in low-calcium E-media to maintain an undifferentiated proliferating state as described previously (69, 70). For collection of conditioned media from keratinocytes for treatment, serum free media was added to confluent plates of cells and conditioned media collected after 16 hours.

Primary newborn dermal fibroblasts were isolated from dermis of P3 pups as described earlier (25). Fibroblasts were cultured in DMEM high-glucose media supplemented with 10% FBS, sodium pyruvate and non-essential amino acids.

Chinese hamster ovarian (CHO) cell line (CHO K1; ATCC CCL-61 ™) was purchased from ATCC. A CHO cell line stably secreting Angiopoietin-like protein 2 was developed by transfecting pcDNA3.1 plasmid containing the mouse *Angptl2* gene. Conditioned media from CHO cells with an empty plasmid was used as control in all the experiments. CHO cells were maintained in DMEM high-glucose media with 10% FBS. For preparation of conditioned media, CHO cells secreting ANGPTL2 and control CHO cells were incubated with media containing 2% FBS for 3 days and the conditioned media collected and snap-frozen before storing at -80°C. For all treatments of SVEC 4-10 endothelial cells this conditioned media was used directly to treat for 48 hours

(for qPCR analysis) and 72 hours (for collagen contraction assay). Concentration of ANGPTL2 for treatments was 500 ng/ml.

Ex-vivo treatment of skin explants and ears

Wild-type adult mouse ears or back skin explants were obtained immediately after sacrificing mice by cervical dislocation, placed in PBS with antibiotics and antifungal drugs (PenStrep, Gentamicin, Fungizone) for 2 hours. Explants were transferred to cell culture plates (dermis side down) containing CHO cell line stably secreting ANGPTL2 or control CHO cells. After 5 days explants were removed and staining and RNA extraction done as described above. For treatments with wildtype and *Snail* tg keratinocyte conditioned media, explants were similarly incubated with respective conditioned media prepared as described previously.

ELISA

The ELISA for ANGPTL2 (Novus biologicals, Cat No: NBP2-68213) was performed on conditioned media (16 hours) from cultured wildtype and *Snail* tg mouse keratinocytes according to the manufacturer's protocols.

Analysis of published datasets for *Angptl2* gene expression

The normalized expression of *Angptl2* in Keloids, SSc, lung with idiopathic pulmonary fibrosis, kidney glomeruli with lupus nephropathy and liver with fibrosis post-transplant was obtained from publicly available microarray data (GSE92566, GSE181549, GSE48149, GSE32591, GSE145780). GEO2R tool (NCBI) was used to analyse the expression level difference between two groups. Welch's t-test used to identify significance level between two groups.

Human samples

SSc patient samples and appropriate control skin samples were obtained from Dr. Vikas Agarwal, Sanjay Gandhi Post Graduate Institute of Medical Sciences, Lucknow, India according to the protocol approved by the Institutional Review Board. Skin-punch biopsies were taken from the arms of patients diagnosed with diffuse systemic sclerosis or nonsystemic sclerosis. Details of patients are listed in Table 2.

Collagen contraction assay

Assay was performed as described previously (71). SVEC 4-10 or SVEC 4-10 cells with claudin5 overexpression were used. Briefly, cells were seeded at a density of 120000 cells in plugs made of Rat tail collagen I (Millipore; 08-115) in a 24-well plate and various treatments added. Collagen plugs were stained with crystal violet and contraction measured from the gel images after 72 hours. The values are represented as fold change of increase in contraction (1/area of collagen gel). Three technical replicates were used for each condition in each biological replicate.

Inhibitor studies

Experiments to inhibit the integrin α5β1 receptor and β-catenin were performed by treating SVEC4-10 cells with ATN-161 (50μM) (TOCRIS, Cat No: 6058/10) and XAV-939 (10μM) (SelleckChem, Cat No: S1180) respectively in the presence of ANGPTL2 for 48 hours (for qPCR analysis) or 72 hours (for collagen contraction assay).

In-vitro permeability assay

FITC-Dextran permeability assay was performed according to previous reports (72, 73). 2 x 10^5 SVEC 4-10 cells were seeded per insert in a 24-well transwell plate and incubated for 72 hours in a 37°C/ 5% CO2 tissue culture incubator to form a confluent monolayer. The growth medium was carefully removed from the inserts so as not to disturb the monolayer and the inserts placed in fresh plate wells. Media containing

Control, ANGPTL2 or UAS03 was added to both inserts (200µl) and wells (500µl) and cells treated for 48 hours in the incubator. The treatment media was removed carefully from the inserts and washed with PBS. The inserts were again placed into fresh well plates containing 500 µl PBS. A working solution of FITC-Dextran (Merck, Cat No: 90718) in PBS (1mg/ml) was prepared and 150 µl added to the inserts. The plate was incubated, protected from light, for 20 minutes at room temperature. Permeation was stopped by removing the inserts from the wells. The media in the wells of the Receiver Tray (now containing FITC-Dextran that crossed the monolayer) was thoroughly mixed. 100 µL of the media from each well of the Receiver Tray was removed and transfered to wells of a black 96-well opaque plate for fluorescence measurement using a fluorescence plate reader with filters appropriate for 485 nm and 535 nm excitation and emission, respectively.

UAS03 treatments

UAS03 formulation was obtained from Dr. Praveen Vemula at inStem, Bangalore, India. For in-vivo experiments, UAS03 (20 mg/kg body weight) was injected interperitoneally once a week starting from post-natal day 3 to 60 when mice were sacrificed. For all in-vitro experiments with SVEC 4-10 cells, 50µM UAS03 in DMSO formulation was used.

Clodronate treatments

Clodronate liposomes (obtained from Anil N. Gaikwad, CSIR-Central Drug Research Institute, Lucknow, India) to deplete macrophages were injected (1 mg) in mice once a week starting from post-natal day 3 to 60 when mice were sacrificed.

RNA Sequencing library preparation and data analysis

RNA was isolated from Control (DMSO) or 50μM UAS03 treated (48 hours) SVEC 4-10 cells (three biological replicates each) as previously described. Integrity of the RNA samples was assessed using the Agilent TapeStation with High Sensitivity RNA ScreenTape. Samples with a RIN greater than 5 were selected for library preparation. mRNA was enriched through oligo-dT bead selection using the Dynabeads mRNA Purification Kit (Invitrogen). The enriched mRNA was then used for downstream library preparation with the MGIEasy RNA Library Prep Kit (MGI, Cat No: 1000005276). Libraries were PCR amplified and circularized using the MGIEasy Circularization Module (MGI, Cat No: 1000005260). These circularized libraries were transformed into DNA Nanoballs (DNBs) and sequenced on the DNBSEQ-G400RS platform using FCL PE100 flow cell chemistry (1000016949 and 1000016985). Approximately, 30–50 million reads were obtained from both control and UAS03 treated samples. The analysis was performed in house following RNA Seq analysis pipeline previously established in the field. FASTQC tool (https://www.bioinformatics.babraham.ac.uk/projects/fastqc/) was used for assessing the quality of Fastq files. Abundance values was generated with kallisto (74) by aligning them against mouse cDNA sequences "Mus_musculus.GRCm39.cdna.all.fa.gz" (https://ftp.ensembl.org/pub/release-113/fasta/mus_musculus/cdna/). The kallisto output was imported in R using tximport and ensDB.MMusculus.v79 database was used for annotation of transcripts. The counts from abundance were calculated using length scaled TPM method. Genes which had count value > 0 in 3 or more samples were selected and normalized using calcNormFactors function using TMM method. Limma and edgeR packages were used to create a linear fit and discover the differentially expressed genes using eBayes function. gplots and ggplot were used for creating the heatmap and volcano plots. Modules containing list of upregulated genes

(q value < 0.05 and Fold Change >1.5) and downregulated genes ((q value < 0.05 and Fold Change >-1.5) were used as input for gProfiler2 (75) for Gene Ontology (GO) term enrichment analysis.

Wounding studies

Twelve-week-old 1) WT mice injected with control or UAS03, or 2) WT and *Angptl2* KO mice were wounded with 5-mm punch biopsies, and wounded skin imaged until complete wound closure. Wound areas were calculated as percentage of the open wound.

Statistics

Comparison of 2 groups was done using either unpaired Welch's t-test (for in-vivo experiments) or paired Students t-test (for in-vitro experiments with cells). Comparison of multiple groups was done using One-way ANOVA followed by Tukey's post hoc analysis. Data are shown as mean ± SEM. GraphPad Prism 5.02 was used for all statistical analyses. P values less than 0.05 were considered significant.

Study approval

Animal work in the Jamora lab was approved by the inStem Institutional Animal Ethics Committee (INS-IAE-2019/06[R1]). Acquisition and processing of the human tissue were conducted according to the protocol approved by the Institutional Review Board of the Sanjay Gandhi Postgraduate Institute of Medical Sciences (Lucknow, India). Informed consent was acquired from all patients for skin sample collection and experimentation. All experimental work was done with approval of the Institutional Biosafety Committee at inStem (inStem/G-141(3)/2012) and Shiv Nadar Institution of Eminence (95/2024).

Data availability

RNA-Seq data for UAS03-treated SVEC 4-10 cells used in this study are deposited in NCBI SRA database BioProject (accession ID PRJNA1207732; http://www.ncbi.nlm.nih.gov/bioproject/1207732). Values for all data points in graphs are reported in the Supporting Data Values file.

Author contributions

DS and CJ conceptualized and designed experiments, evaluated and interpreted data, and wrote the manuscript. DS, RK, ST, NP, SK, BD, AD, Akshay Hegde, Ankita Hiwale, VR and SS performed experiments. DS, RK and ST acquired and analysed data. SK performed bioinformatics analysis, acquired and analysed data. LMR, NN, NS and VA provided resources (SSc samples). PKV provided resources (UAS03) and guidance for experimental design. CJ provided guidance and acquired funding.

Acknowledgments

The authors would like to thank members of the Jamora laboratory and John Varga for critical review of the manuscript and Krithika Badarinath for technical assistance. We thank Srikala Raghavan, Tina Mukherjee and Maneesha Inamdar for insightful discussions. Clodronate liposomes were a gift from Anil N. Gaikwad (CSIR-Central Drug Research Institute, Lucknow). This work was supported by core funds from inStem and Shiv Nadar Institution of Eminence and grants from the Department of Biotechnology of the Government of India (BT/PR8738/AGR/36/770/2013, BT/PR32539/BRB/10/1814/2019) and the Indian Council of Medical Research (IIRPIG-2024-01-01387). Animal studies were partially supported by the National Mouse Research Resource grant BT/ PR5981/MED/31/181/2012;2013-2016;2018 and 102/IFD/SAN/5003/2017- 2018 from the Department of Biotechnology. We thank the staff of the Animal Care and Resource Centre and Mouse Genome Engineering Facility (Aurelie Jory, Vaishak Nair Penar, B. Sangeetha, Lalitha K S) and the Central Imaging and Flow Cytometry Facility at the Bangalore Life Science Cluster. We thank Dr. Sanjeev Galande (Center of Excellence in Epigenetics, Department of Life Sciences, Shiv Nadar Institution of Eminence) for help with transcriptome profiling and

creation of models using BioRender. We also thank the Core Imaging facility (Rajan Singh) at Shiv Nadar Institution of Eminence which was supported in part by a DST-FIST grant (SR/FST/LS-1/2017/59(c)). The graphical abstract and summary model (Figure 9) were created using BioRender.com.

REFERENCES

1. Wynn TA. Common and unique mechanisms regulate fibrosis in various fibroproliferative diseases. *J Clin Invest*. 2007;117(3):524.

2. Frangogiannis NG. Transforming growth factor–ß in tissue fibrosis. *J Exp Med*. 2020;217(3). https://doi.org/10.1084/JEM.20190103/133821.

3. Huang E, et al. The Roles of Immune Cells in the Pathogenesis of Fibrosis. *Int J Mol Sci*. 2020;21(15):1–27.

4. Connolly MK. Systemic sclerosis (scleroderma): remaining challenges. *Ann Transl Med*. 2021;9(5):438–438.

5. Careta MF, Romiti R. Localized scleroderma: clinical spectrum and therapeutic update. *An Bras Dermatol*. 2015;90(1):62.

6. Sobolewski P, et al. Systemic sclerosis – multidisciplinary disease: clinical features and treatment. *Reumatologia*. 2019;57(4):221.

7. Pattanaik D, Brown M, Postlethwaite AE. Vascular involvement in systemic sclerosis (scleroderma). *J Inflamm Res*. 2011;4(1):105.

8. Matucci-Cerinic M, Kahaleh B, Wigley FM. Review: Evidence That Systemic Sclerosis Is a Vascular Disease. *Arthritis Rheum*. 2013;65(8):1953–1962.

9. Rosendahl AH, Schönborn K, Krieg T. Pathophysiology of systemic sclerosis (scleroderma). *Kaohsiung J Med Sci*. 2022;38(3):187–195.

10. Singh D, et al. Scleroderma: An insight into causes, pathogenesis and treatment strategies. *Pathophysiology*. 2019;26(2):103–114.

11. Artlett CM. Animal models of systemic sclerosis: their utility and limitations. *Open*

Access Rheumatol Res Rev. 2014;6:65.

12. Yue X, et al. Recent advances in mouse models for systemic sclerosis. *Autoimmun Rev*. 2018;17(12):1225–1234.

13. Christner PJ, et al. The tight skin 2 mouse. *Arthritis Rheum*. 1995;38(12):1791–1798.

14. Gentiletti J, et al. Demonstration of autoimmunity in the tight skin-2 mouse: a model for scleroderma. *J Immunol*. 2005;175(4):2418–2426.

15. Wong AK, et al. Quantification of ventricular remodeling in the tight-skin mouse cardiomyopathy with acoustic microscopy. *Ultrasound Med Biol*. 1993;19(5):365–374.

16. Murai C, et al. Spontaneous occurrence of anti-fibrillin-1 autoantibodies in tight-skin mice. *Autoimmunity*. 1998;28(3):151–155.

17. Błyszczuk P, et al. Experimental Mouse Model of Bleomycin-Induced Skin Fibrosis. *Curr Protoc Immunol*. 2019;126(1):e88.

18. Yamamoto T, Katayama I. Vascular changes in bleomycin-induced scleroderma. *Int J Rheumatol*. 2011;2011. https://doi.org/10.1155/2011/270938.

19. Boutet A, et al. Snail activation disrupts tissue homeostasis and induces fibrosis in the adult kidney. *EMBO J*. 2006;25(23):5603–5613.

20. Goyal A, et al. Differential Expression of Hedgehog and Snail in Cutaneous Fibrosing Disorders: Implications for Targeted Inhibition. *Am J Clin Pathol*. 2016;146(6):709–717.

21. Jayachandran A, et al. SNAI transcription factors mediate epithelial–

mesenchymal transition in lung fibrosis. *Thorax*. 2009;64(12):1053–1061.

22. Rowe RG, et al. Hepatocyte-Derived Snail1 Propagates Liver Fibrosis Progression. *Mol Cell Biol*. 2011;31(12):2392.

23. Rana I, et al. Mindin (SPON2) Is Essential for Cutaneous Fibrogenesis in a Mouse Model of Systemic Sclerosis. *J Invest Dermatol*. [published online ahead of print: December 15, 2022]. https://doi.org/10.1016/J.JID.2022.10.011.

24. Pincha N, et al. PAI1 mediates fibroblast–mast cell interactions in skin fibrosis. *J Clin Invest*. 2018;128(5):1807–1819.

25. Nakasaki M, et al. The matrix protein Fibulin-5 is at the interface of tissue stiffness and inflammation in fibrosis. *Nat Commun*. 2015;6(1):8574.

26. Asano Y, Sato S. Vasculopathy in scleroderma. *Semin Immunopathol*. 2015;37(5):489–500.

27. Nakamura K, et al. Altered properties of endothelial cells and mesenchymal stem cells underlying the development of scleroderma-like vasculopathy in *Klf5* $^{+/-}$; *Fli1* $^{+/-}$ mice. *Arthritis Rheumatol*. 2020;art.41423.

28. Manetti M, et al. Endothelial-to-mesenchymal transition contributes to endothelial dysfunction and dermal fibrosis in systemic sclerosis. *Ann Rheum Dis*. 2017;76(5):924–934.

29. Hadi HAR, Carr CS, Al Suwaidi J. Endothelial Dysfunction: Cardiovascular Risk Factors, Therapy, and Outcome. *Vasc Health Risk Manag*. 2005;1(3):183.

30. Salani D, et al. Endothelin-1 Induces an Angiogenic Phenotype in Cultured Endothelial Cells and Stimulates Neovascularization In Vivo. *Am J Pathol*. 2000;157(5):1703–1711.

31. Iwayama T, Olson LE. Involvement of PDGF in fibrosis and scleroderma: recent insights from animal models and potential therapeutic opportunities. *Curr Rheumatol Rep*. 2013;15(2). https://doi.org/10.1007/S11926-012-0304-0.

32. Schwartz MA, Vestweber D, Simons M. Blood vessel stability vs. instability: a unifying concept in vascular health and disease. https://doi.org/10.1126/science.aat3470.

33. Platel V, et al. Endothelial-to-Mesenchymal Transition (EndoMT): Roles in Tumorigenesis, Metastatic Extravasation and Therapy Resistance. *J Oncol*. 2019;2019. https://doi.org/10.1155/2019/8361945.

34. Piera-Velazquez S, Mendoza FA, Jimenez SA. Endothelial to Mesenchymal Transition (EndoMT) in the Pathogenesis of Human Fibrotic Diseases. *J Clin Med*. 2016;5(4). https://doi.org/10.3390/JCM5040045.

35. Fuentes-Duculan J, et al. Aberrant connective tissue differentiation towards cartilage and bone underlies human keloids in African Americans. *Exp Dermatol*. 2017;26(8):721–727.

36. Skaug B, et al. Large-scale analysis of longitudinal skin gene expression in systemic sclerosis reveals relationships of immune cell and fibroblast activity with skin thickness and a trend towards normalization over time. *Ann Rheum Dis*. 2022;81(4):516.

37. Hsu E, et al. Lung tissues in patients with systemic sclerosis have gene expression patterns unique to pulmonary fibrosis and pulmonary hypertension. *Arthritis Rheum*. 2011;63(3):783–794.

38. Berthier CC, et al. Cross-species transcriptional network analysis defines shared

inflammatory responses in murine and human lupus nephritis. *J Immunol*. 2012;189(2):988–1001.

39. Madill-Thomsen K, et al. The molecular diagnosis of rejection in liver transplant biopsies: First results of the INTERLIVER study. *Am J Transplant*. 2020;20(8):2156–2172.

40. Endo M, et al. Tumor cell-derived angiopoietin-like protein ANGPTL2 is a critical driver of metastasis. *Cancer Res*. 2012;72(7):1784–1794.

41. Derada Troletti C, et al. Inflammation-induced endothelial to mesenchymal transition promotes brain endothelial cell dysfunction and occurs during multiple sclerosis pathophysiology. *Cell Death Dis 2019 102*. 2019;10(2):1–13.

42. Ciszewski WM, et al. Cytoskeleton Reorganization in EndMT—The Role in Cancer and Fibrotic Diseases. *Int J Mol Sci*. 2021;22(21):11607.

43. Chiu Y-H, et al. Association of endothelial to mesenchymal transition and cellular senescence with fibrosis in skin biopsies of systemic sclerosis patients: a cross-sectional study. *Clin Exp Rheumatol*. [published online ahead of print: August 30, 2022]. https://doi.org/10.55563/clinexprheumatol/i49d3o.

44. Richards M, et al. Claudin5 protects the peripheral endothelial barrier in an organ and vessel-type-specific manner. *Elife*. 2022;11. https://doi.org/10.7554/ELIFE.78517.

45. Greene C, et al. Microvascular stabilization via blood-brain barrier regulation prevents seizure activity. *Nat Commun*. 2022;13(1). https://doi.org/10.1038/S41467-022-29657-Y.

46. Tabata M, et al. Angiopoietin-like Protein 2 Promotes Chronic Adipose Tissue

Inflammation and Obesity-Related Systemic Insulin Resistance. *Cell Metab*. 2009;10(3):178–188.

47. Sabbineni H, et al. Pharmacological inhibition of β-catenin prevents EndMT in vitro and vascular remodeling in vivo resulting from endothelial Akt1 suppression. *Biochem Pharmacol*. 2019;164:205–215.

48. Singh R, et al. Enhancement of the gut barrier integrity by a microbial metabolite through the Nrf2 pathway. *Nat Commun*. 2019;10(1):89.

49. Parri M, et al. Angiopoietin-like 7, a novel pro-angiogenetic factor over-expressed in cancer. *Angiogenesis*. 2014;17(4):881–896.

50. Ma YS, et al. KDM5A silencing transcriptionally suppresses the FXYD3-PI3K/AKT axis to inhibit angiogenesis in hepatocellular cancer via miR-433 up-regulation. *J Cell Mol Med*. 2021;25(8):4040.

51. Konno Y, et al. The Nuclear Receptors Constitutive Active/Androstane Receptor and Pregnane X Receptor Activate the Cyp2c55 Gene in Mouse Liver. *Drug Metab Dispos*. 2010;38(7):1177.

52. Lertkiatmongkol P, et al. Endothelial functions of platelet/endothelial cell adhesion molecule-1 (CD31). *Curr Opin Hematol*. 2016;23(3):253–259.

53. Matucci-Cerinic M, et al. The “myth” of loss of angiogenesis in systemic sclerosis: a pivotal early pathogenetic process or just a late unavoidable event? *Arthritis Res Ther*. 2017;19(1). https://doi.org/10.1186/S13075-017-1370-5.

54. Shenavandeh S, et al. Serum vascular endothelial growth factor (VEGF), soluble VEGF receptor-1 (sVEGFR-1) and sVEGFR-2 in systemic sclerosis patients: Relation to clinical manifestations and capillaroscopy findings. *Egypt Rheumatol*.

2017;39(1):19–24.

55. Du F, et al. Expression of Snail in epidermal keratinocytes promotes cutaneous inflammation and hyperplasia conducive to tumor formation. *Cancer Res*. 2010;70(24):10080.

56. Viallard C, Larrivée B. Tumor angiogenesis and vascular normalization: alternative therapeutic targets. *Angiogenesis*. 2017;20(4):409–426.

57. Ramirez GA, et al. The role of platelets in the pathogenesis of systemic sclerosis. *Front Immunol*. 2012;3(JUN). https://doi.org/10.3389/FIMMU.2012.00160.

58. Nurden AT. Platelets, inflammation and tissue regeneration. *Thromb Haemost*. 2011;105(SUPPL. 1):13–33.

59. Varga J, Abraham D. Systemic sclerosis: a prototypic multisystem fibrotic disorder. *J Clin Invest*. 2007;117(3):557–567.

60. Hashizume H, et al. Openings between Defective Endothelial Cells Explain Tumor Vessel Leakiness. *Am J Pathol*. 2000;156(4):1363–1380.

61. BURKE JF, MILES AA. The sequence of vascular events in early infective inflammation. *J Pathol Bacteriol*. 1958;76(1):1–19.

62. Thorin-Trescases N, Thorin E. High Circulating Levels of ANGPTL2: Beyond a Clinical Marker of Systemic Inflammation. *Oxid Med Cell Longev*. 2017;2017. https://doi.org/10.1155/2017/1096385.

63. Kubota Y, et al. Cooperative interaction of Angiopoietin-like proteins 1 and 2 in vascular development. *Proc Natl Acad Sci U S A*. 2005;102(38):13502–13507.

64. Wang X, et al. Angiopoietin-like protein 2 is an important facilitator of tumor

proliferation, metastasis, angiogenesis and glycolysis in osteosarcoma. *Am J Transl Res*. 2019;11(10):6341.

65. Masuda T, et al. ANGPTL2 increases bone metastasis of breast cancer cells through enhancing CXCR4 signaling. *Sci Rep*. 2015;5:9170–9170.

66. Enevoldsen FC, et al. Endothelin Receptor Antagonists: Status Quo and Future Perspectives for Targeted Therapy. *J Clin Med*. 2020;9(3). https://doi.org/10.3390/JCM9030824.

67. Van Le TH, Kwon SM. Vascular Endothelial Growth Factor Biology and Its Potential as a Therapeutic Target in Rheumatic Diseases. *Int J Mol Sci 2021, Vol 22, Page 5387*. 2021;22(10):5387.

68. Jamora C, et al. A Signaling Pathway Involving TGF-β2 and Snail in Hair Follicle Morphogenesis. *PLoS Biol*. 2004;3(1):e11.

69. Nowak JA, Fuchs E. Isolation and culture of epithelial stem cells. *Methods Mol Biol*. 2009;482:215–232.

70. Bhatt T, et al. Initiation of wound healing is regulated by the convergence of mechanical and epigenetic cues. *PLOS Biol*. 2022;20(9):e3001777.

71. Pincha N, et al. Activation of Fibroblast Contractility via Cell-Cell Interactions and Soluble Signals. *BIO-PROTOCOL*. 2018;8(18). https://doi.org/10.21769/BioProtoc.3021.

72. Miyazaki K, et al. Establishment of a method for evaluating endothelial cell injury by TNF-α in vitro for clarifying the pathophysiology of virus-associated acute encephalopathy. *Pediatr Res*. 2017;81(6):942–947.

73. Simoneau B, Houle F, Huot J. Regulation of endothelial permeability and

transendothelial migration of cancer cells by tropomyosin-1 phosphorylation. *Vasc Cell*. 2012;4:18.

74. Bray NL, et al. Near-optimal probabilistic RNA-seq quantification. *Nat Biotechnol 2016 345*. 2016;34(5):525–527.

75. Kolberg L, et al. g:Profiler—interoperable web service for functional enrichment analysis and gene identifier mapping (2023 update). *Nucleic Acids Res*. 2023;51(W1):W207–W212.

FIGURES

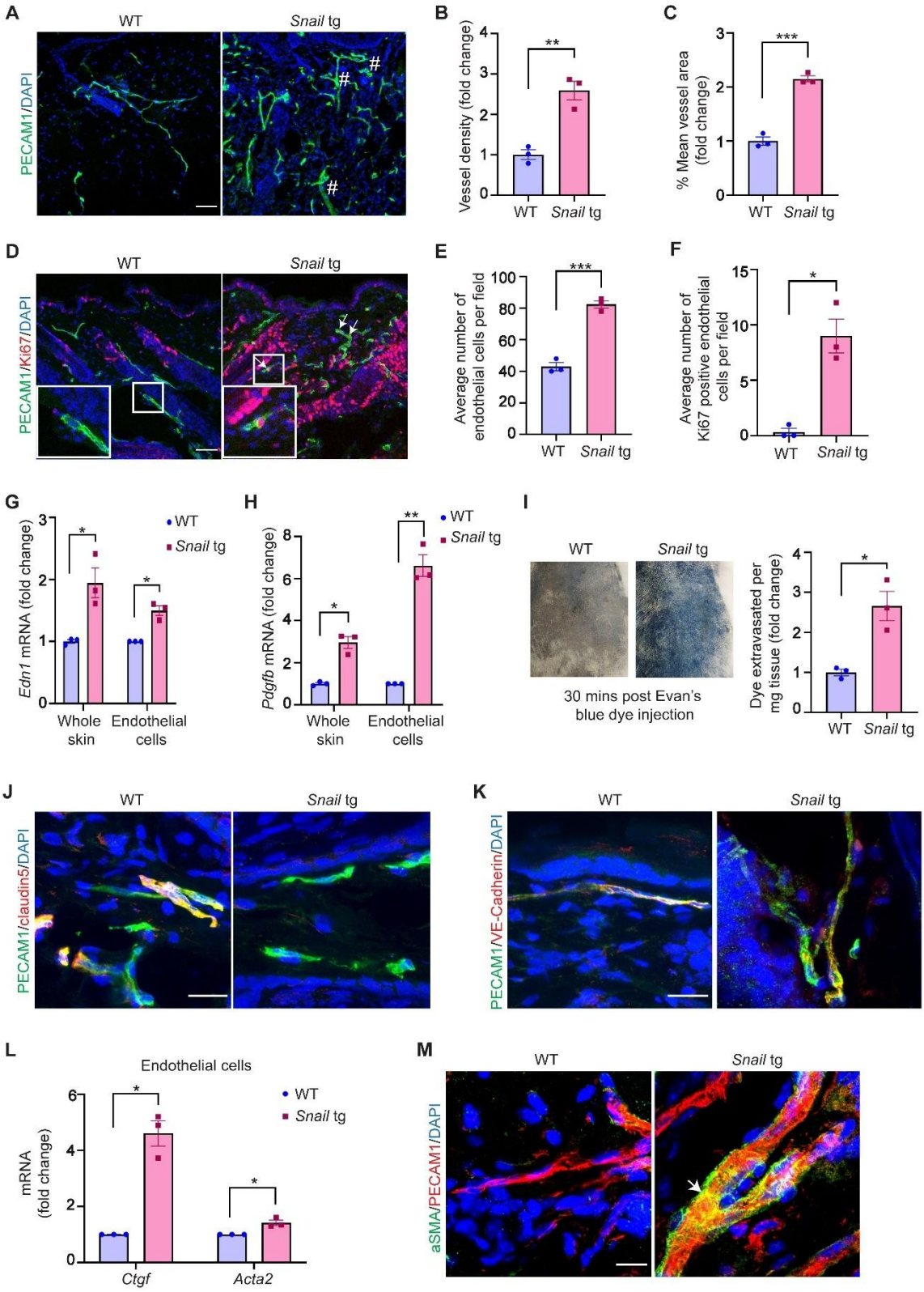

Figure 1: Adult *Snail* tg skin recapitulates vasculature abnormalities observed in SSc. (A) Wild type (WT) and *Snail* tg skin stained for PECAM1 (green). Dilated regions of vessels

are denoted with a #. Quantification of (B) vessel density and (C) mean vessel area in WT and *Snail* tg skin. (D) WT and *Snail* tg skin stained for PECAM1 (green) and proliferation marker Ki67 (red). Arrows mark PECAM1$^+$/Ki67$^+$ cells. Inset shows magnified endothelial cell. Number of (E) endothelial cells and (F) PECAM1$^+$/Ki67$^+$ cells in WT and *Snail* tg skin. qPCR analysis of (G) *Edn1* mRNA and (H) *Pdgfb* mRNA in whole skin and isolated dermal endothelial cells in WT and *Snail* tg mice. (I) Evan's blue dye leakage assay and quantification. WT and *Snail* tg skin stained for (J) Claudin5 (red)/PECAM1 (green) and (K) VE-Cadherin (red)/PECAM1(green). (L) qPCR analysis of myofibroblast markers (*Ctgf*, *Acta2*) in isolated dermal endothelial cells from WT and *Snail* tg mice skin. (M) WT and *Snail* tg skin stained for αSMA (green) and PECAM1 (red). Arrow marks αSMA$^+$/PECAM1$^+$ vascular structure. Nuclei are marked in blue. Scale bars: 50 μm for (A), (D); 20 μm for (J), (K);10 μm for (M). Data are shown as mean ± SEM, p-values were calculated using unpaired Welch's t test for whole skin data and paired student t-test for endothelial cell data, * $p < 0.05$, ** $p < 0.01$, *** $p < 0.001$. All experiments are n=3 biological replicates. 3 fields of interest (FOI) were analysed per biological replicate for quantification of images.

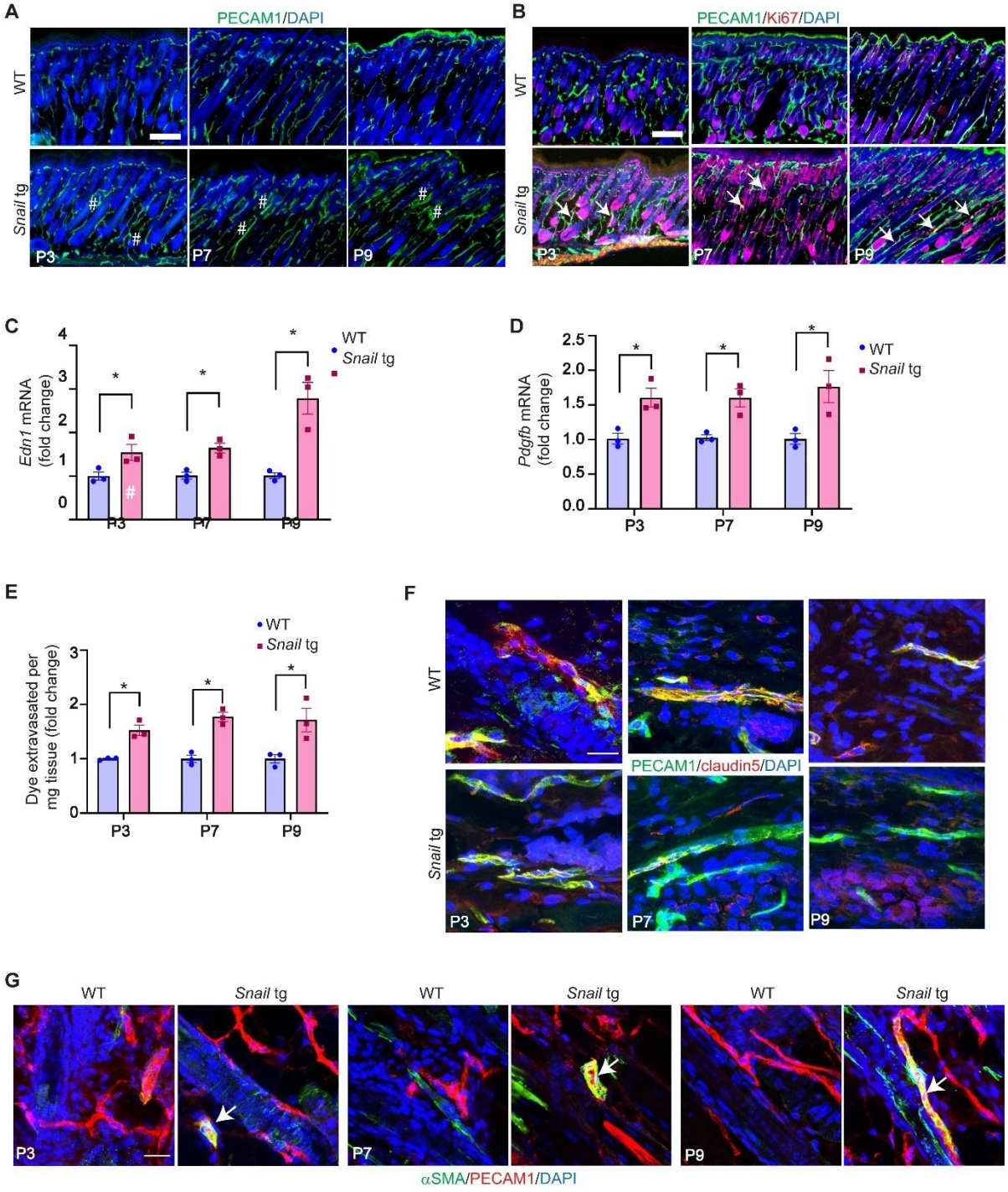

Figure 2: Vasculopathy phenotype occurs early in fibrogenesis. The skin from postnatal day 3, 7, and 9 wild type (WT) and *Snail* tg mice were stained for (A) PECAM1 (green) and (B) PECAM1 (green) and Ki67 (red). Dilated regions are marked by # and arrows mark PECAM1^{+}/Ki67^{+} cells. qPCR analysis of (C) *Edn1* mRNA and (D) *Pdgfb* mRNA in whole skin in WT and *Snail* tg mice. (E) Quantification of Evan's blue dye leakage assay. WT and *Snail* tg skin stained for (F) claudin5 (red) and PECAM1 (green); and (G) αSMA (green) and PECAM1(red). Arrow marks αSMA/PECAM1 double positive vascular structure. Nuclei are marked in blue. Scale bars: 100μm for (A) and (B); 20μm for (F) and (G). Data are shown as

mean ± SEM, p-values were calculated using unpaired Welch's t test, * $p < 0.05$. All experiments are n=3 biological replicates.

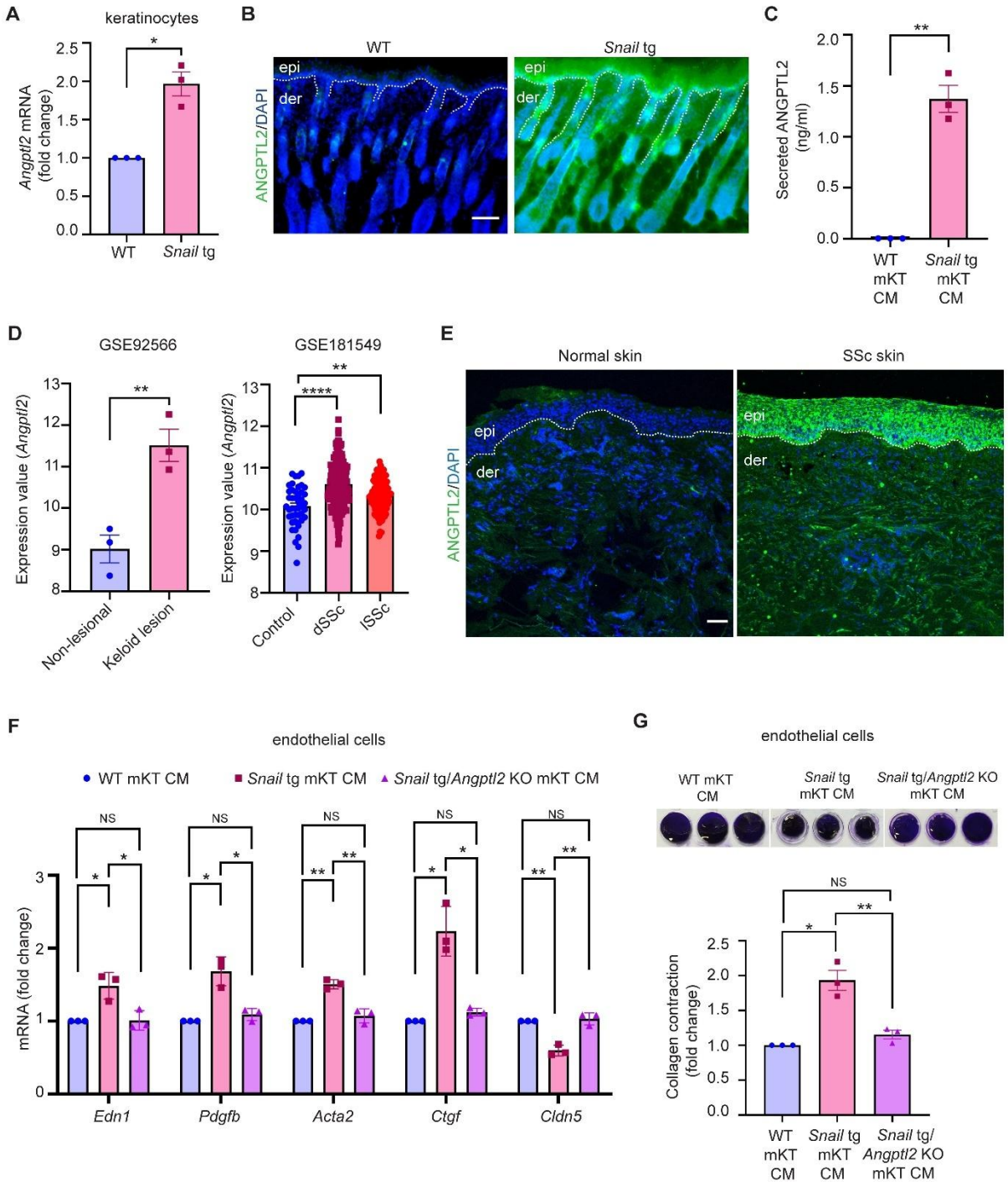

Figure 3: ANGPTL2 is necessary for fibrotic vasculopathy. (A) qPCR of *Angptl2* mRNA in wildtype (WT) and *Snail* tg mouse keratinocytes (mKT). (B) Secreted ANGPTL2 (in green) in WT and *Snail* tg skin at P3. The dotted line denotes the basement membrane separating the epidermis (epi) from the underlying dermis (der). (C) ELISA for secreted ANGPTL2 in WT and *Snail* tg mKT conditioned media. (D) Expression of *Angptl2* in keloid lesion skin (n=3) compared to non-lesional skin (n=3) (from GSE92566) and in healthy (n=44) compared to affected forearm skin from diffuse (n=180) and localized SSc (n=115) patients (from GSE181549). The expression values are fetched from the GEO2R algorithm's output. (E)

Secreted ANGPTL2 (in green) in normal and systemic sclerosis (SSc) skin. Representative of n=5 SSc samples and normal skin controls. (F) qPCR of vasculopathy and endoMT related genes in SVEC4-10 endothelial cells treated with WT, *Snail* tg and *Snail* tg /*Angptl2* KO mKT conditioned media. (G) Quantification of collagen contraction assay in SVEC4-10 endothelial cells treated with WT, *Snail* tg and *Snail* tg /*Angptl2* KO mKT conditioned media. Nuclei are marked in blue. Scale bar: 50 μm. Data are shown as mean ± SEM, p-values were calculated using paired student T test (A), Welch's t test (D) and one-way ANOVA followed by Tukey's post hoc analysis (F and G). * $p < 0.05$, ** $p < 0.01$, **** $p < 0.0001$, NS > 0.05. All experiments except (D) and (E) are n=3 biological replicates.

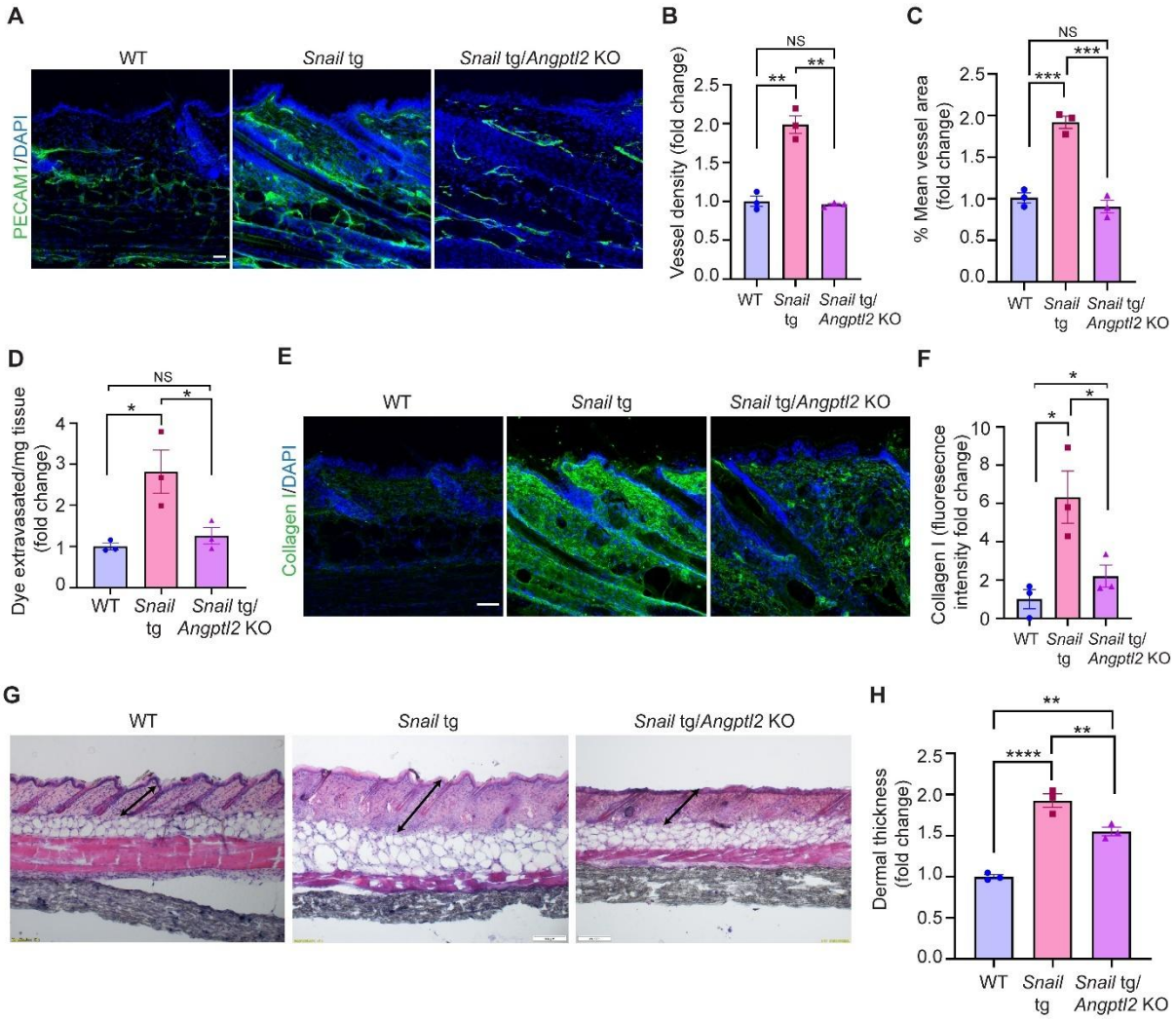

Figure 4: ANGPTL2 is required for development of vasculopathy and fibrosis in the *Snail* tg skin. (A) PECAM1 (green) staining, (B) quantification of vessel density, (C) quantification of vessel area, (D) quantification of Evan's blue dye leakage assay, (E) Collagen I staining (green) and (F) quantification, and (G) H/E staining and (H) quantification of dermal thickness in wildtype (WT), *Snail* tg and *Snail* tg/*Angptl2* KO mouse at P60. Scale bar: 50 µm for (A), (E), and 100 µm for (G). Nuclei are marked in blue. Data are shown as mean ± SEM, p-values were calculated using one-way ANOVA followed by Tukey's post hoc analysis for multiple group comparisons. * $p < 0.05$, ** $p < 0.01$, *** $p < 0.001$, **** $p < 0.0001$, NS > 0.05. All experiments are n=3 biological replicates. 3 FOI were analysed per biological replicate for quantification of images.

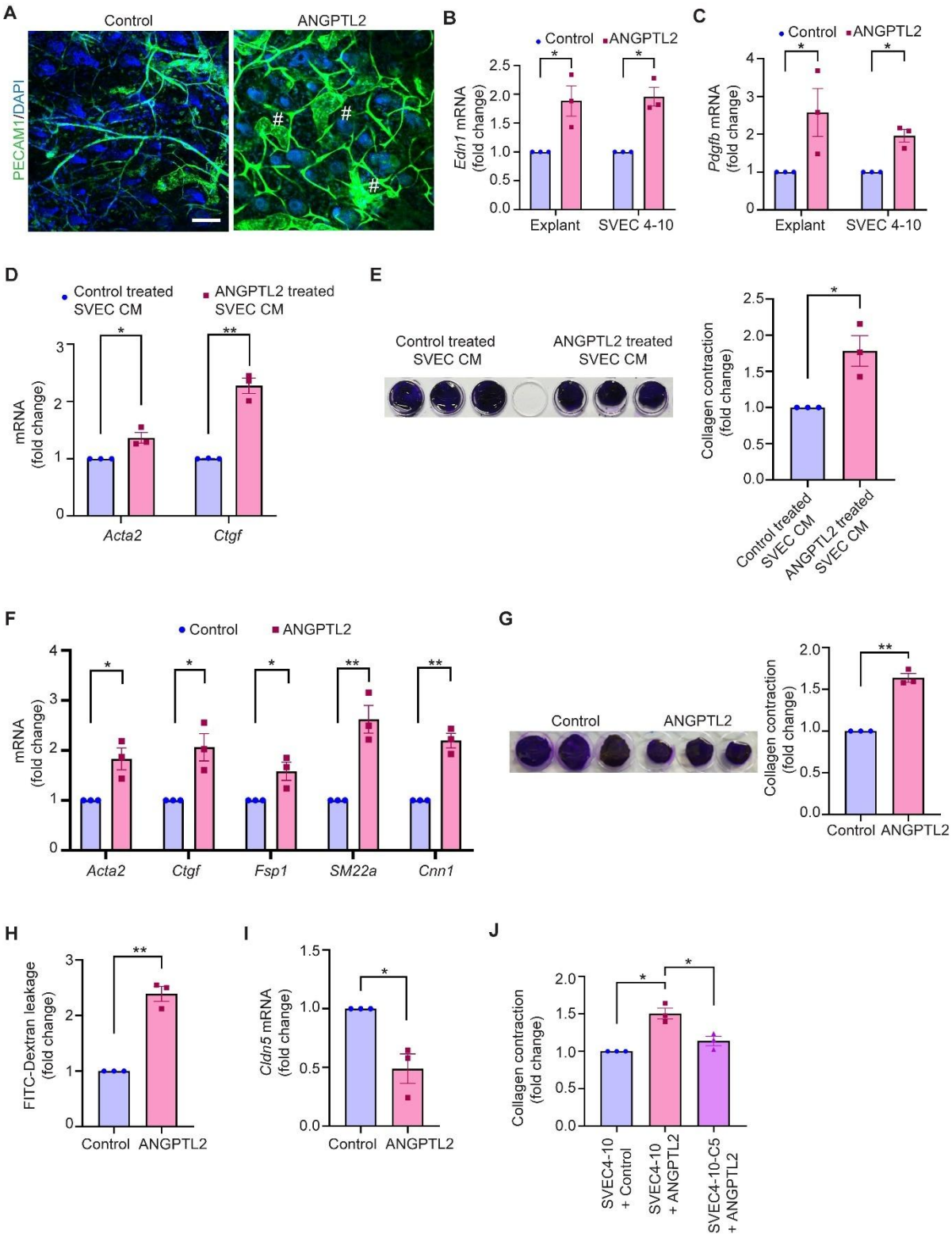

Figure 5: ANGPTL2 is sufficient to drive vasculopathy. (A) PECAM1 (green) staining in control and ANGPTL2 treated skin explants. # denotes dilated regions. Nuclei are marked in blue. qPCR analysis of mRNA levels of (B) *Edn1* and (C) *Pdgfb* in control and ANGPTL2 treated skin explants and SVEC 4-10 cells. (D) qPCR analysis of mRNA levels of

myofibroblasts markers (*Acta2*,*Ctgf*) and (E) Collagen contraction assay (left panel) and quantification (right panel) using dermal fibroblasts treated with conditioned media from control and ANGPTL2 treated SVEC 4-10 cells. (F) qPCR analysis of mRNA levels of myofibroblasts markers (*Acta2*, *Ctgf*, *Fsp1*. *SM22a*, *Cnn1*) in control and ANGPTL2 treated SVEC 4-10. (G) Collagen contraction assay (left panel) and quantification (right panel) for control and ANGPTL2 treated SVEC 4-10. (H) Quantification of in-vitro vascular permeability assay. (I) qPCR analysis of mRNA levels of *Cldn5* in control and ANGPTL2 treated SVEC 4-10. (J) Quantification of collagen contraction assay in SVEC4-10 + Control, SVEC4-10 + ANGPTL2, and claudin5 overexpressed SVEC4-10 (SVEC 4-10-C5) + ANGPTL2. Scale bar: 50 μm. Data are shown as mean ± SEM, p-values were calculated using paired student t-test (B-I) and one-way ANOVA followed by Tukey's post hoc analysis (J). * $p < 0.05$, ** $p < 0.01$. All experiments are n=3 biological replicates.

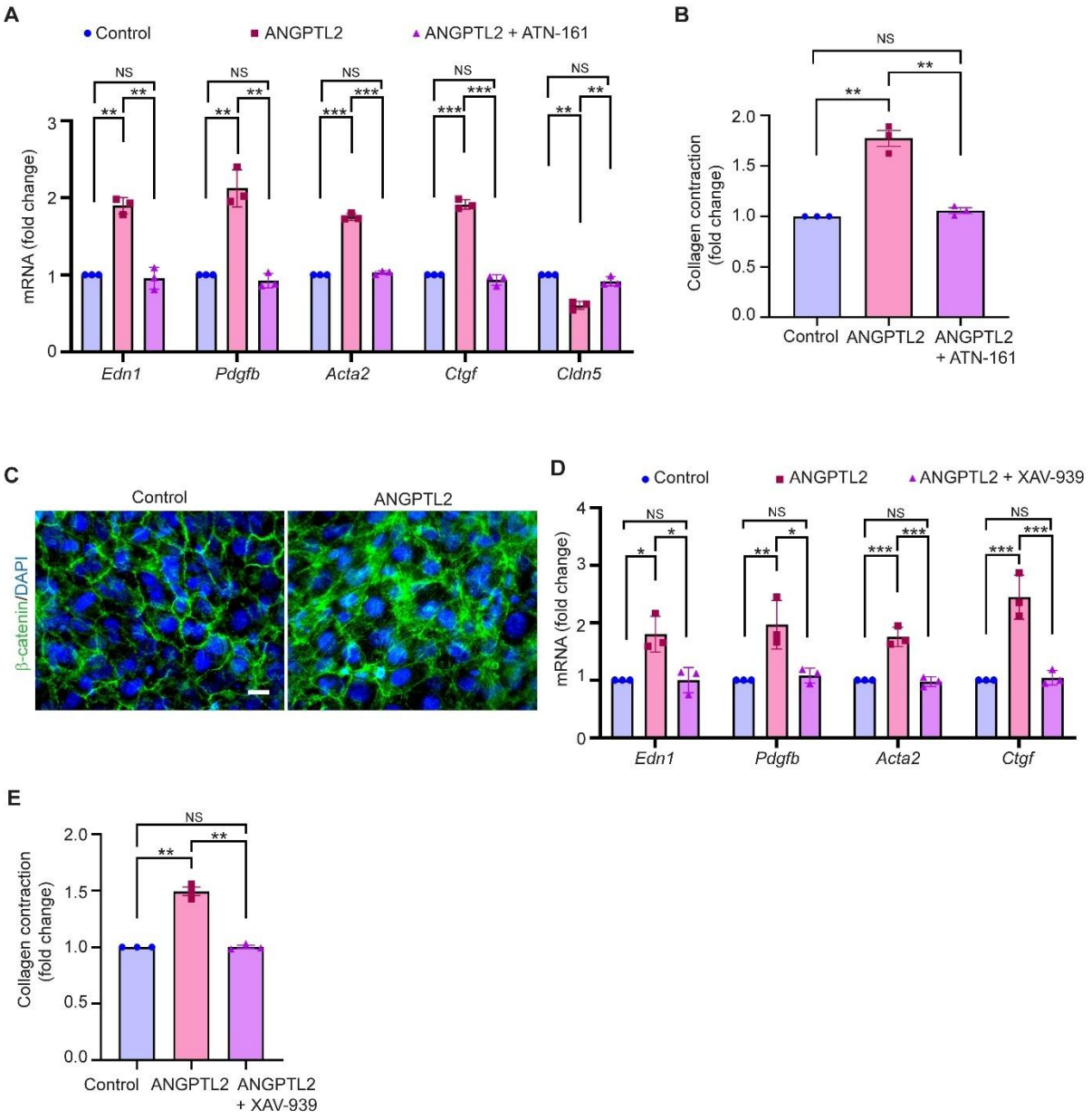

Figure 6: ANGPTL2 driven vasculopathy is mediated by the integrin α5β1-β catenin pathway. (A) qPCR analysis of mRNA levels of vasculopathy and endoMT related genes and (B) Collagen contraction assay quantification in SVEC 4-10 cells treated with Control, ANGPTL2 and ANGPTL2 + ATN-161. (C) Staining for β-catenin (green) in Control or ANGPTL2 treated SVEC 4-10 cells. (D) qPCR analysis of mRNA levels of vasculopathy and endoMT related genes; and (E) Collagen contraction assay quantification in SVEC 4-10 cells treated with Control, ANGPTL2 and ANGPTL2 + XAV-939. Scale bar: 10 μm. Data are shown as mean ± SEM, p-values were calculated using one-way ANOVA followed by Tukey's post hoc analysis for multiple group comparisons. * $p < 0.05$, ** $p < 0.01$, *** $p < 0.001$, NS > 0.05. All experiments are n=3 biological replicates.

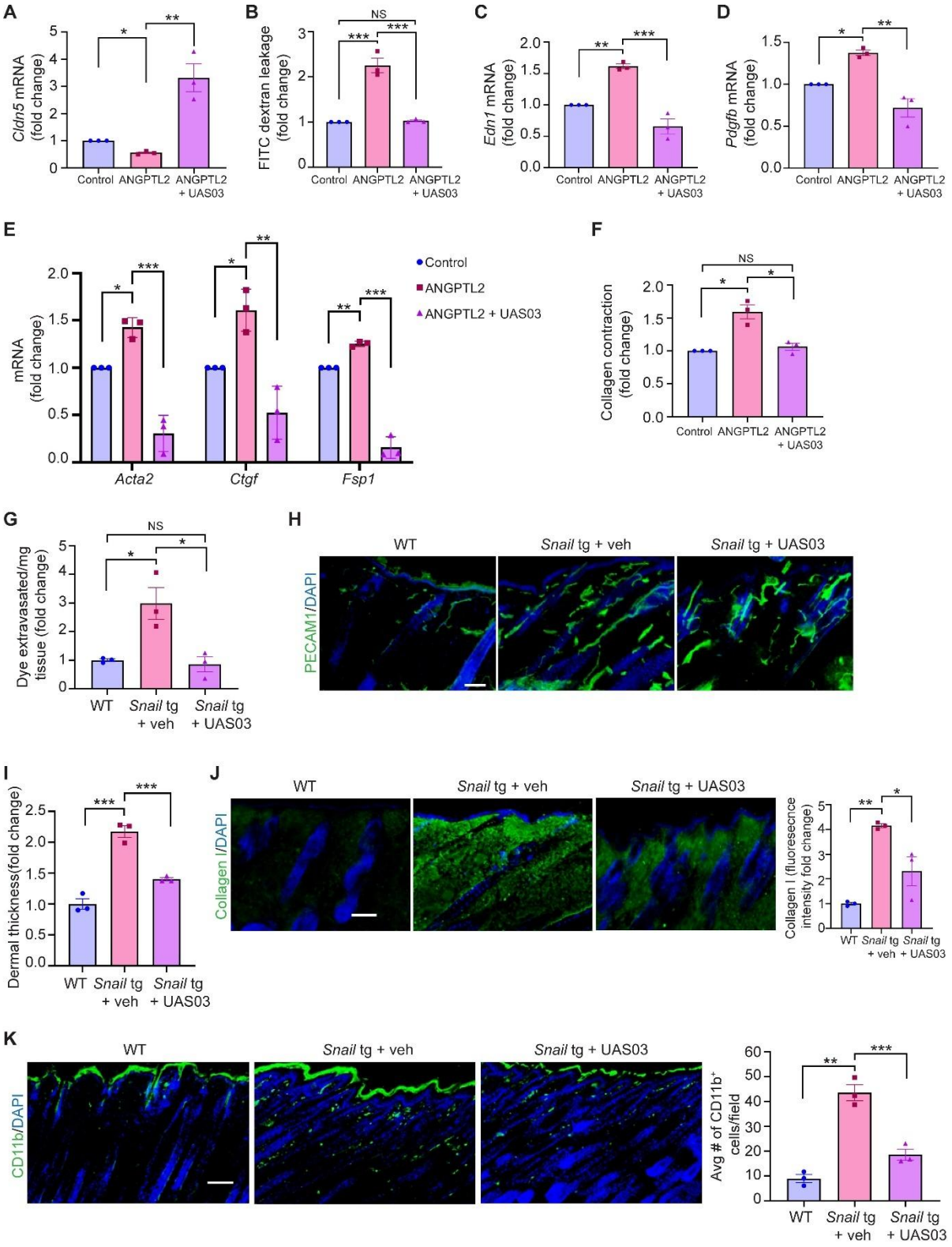

Figure 7: UAS03 abrogates effects of ANGPTL2 on endothelial cells and counteracts fibrosis. SVEC 4-10 cells were treated with control, ANGPTL2, or ANGPTL2 + UAS03 and processed for qPCR of *Cldn5* mRNA (A); in vitro vascular permeability (B); qPCR of *Edn1* mRNA (C), qPCR of *Pdgfb* mRNA (D); expression of myofibroblast markers (*Acta2*, *Ctgf*, *Fsp1*)

(E) and collagen contraction activity (F). (G) Quantification of Evan's blue dye leakage assay. (H) Staining for PECAM1 (green) and nuclei (DAPI) at P60 in wild type (WT), *Snail* tg + vehicle control (veh) and *Snail* tg + UAS03 injected mice. (I) Quantification of dermal thickness at P60 in WT, *Snail* tg + veh and *Snail* tg + UAS03. (J) Staining for Collagen I (green) and quantification at P60 in WT, *Snail* tg + veh and *Snail* tg + UAS03. (K) Staining for CD11b+ cells (green) and nuclei (blue) and quantification at P9 in WT, *Snail* tg + veh and *Snail* tg + UAS03. Scale bar: 100 μm for (H) and (I), 50 μm for (K). Data are shown as mean ± SEM, p-values were calculated using paired Student's t test for (A) - (F) and one-way ANOVA followed by Tukey's post hoc analysis for multiple group comparisons for (G), (I)-(K), * $p < 0.05$, ** $p < 0.01$, *** $p < 0.001$, NS > 0.05. All experiments are n=3 biological replicates. 3 FOI were analysed per biological replicate for quantification of images.

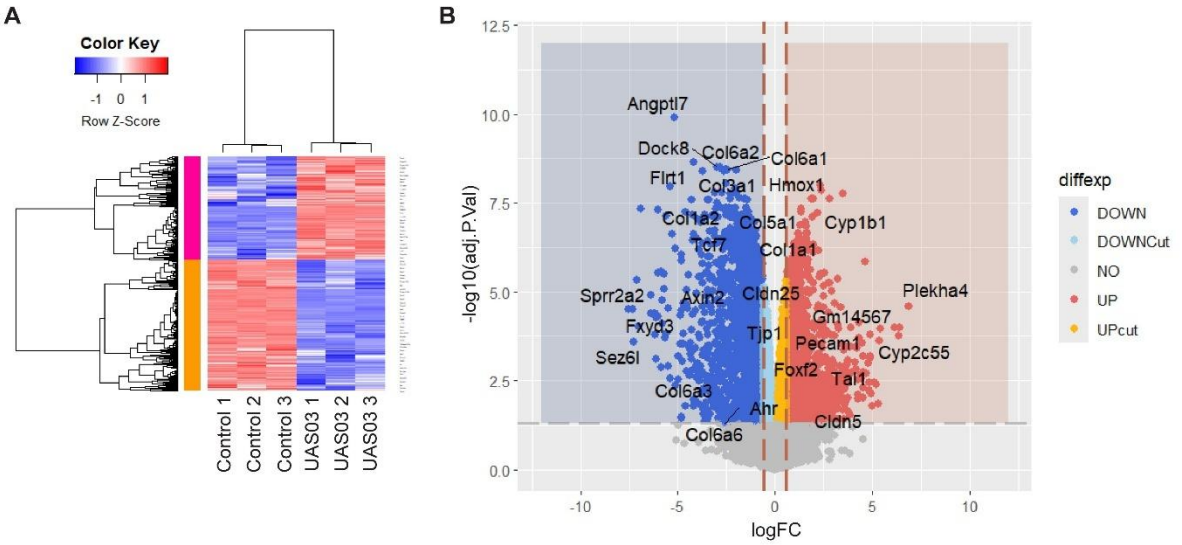

C

ID	Source	Term ID	Term Name	p_{adj} (query_1)
5	GO:BP	GO:0006950	response to stress	6.940×10^{-15}
6	GO:BP	GO:0019222	regulation of metabolic process	4.423×10^{-13}
8	GO:BP	GO:0007166	cell surface receptor signaling pathway	5.948×10^{-10}
7	GO:BP	GO:0033554	cellular response to stress	6.770×10^{-10}
9	GO:BP	GO:0051716	cellular response to stimulus	1.109×10^{-9}
10	GO:BP	GO:0023051	regulation of signaling	9.572×10^{-9}
11	GO:BP	GO:0006974	DNA damage response	4.882×10^{-7}
1	GO:MF	GO:0140110	transcription regulator activity	5.554×10^{-4}
2	GO:MF	GO:0001216	DNA-binding transcription activator activity	2.975×10^{-3}
3	GO:MF	GO:0019899	enzyme binding	1.026×10^{-2}
4	GO:MF	GO:0008330	protein tyrosine/threonine phosphatase activity	4.282×10^{-2}

D

ID	Source	Term ID	Term Name	p_{adj} (query_1)
1	GO:BP	GO:0001944	vasculature development	8.159×10^{-45}
2	GO:BP	GO:0001525	angiogenesis	5.704×10^{-29}
3	GO:BP	GO:0030198	extracellular matrix organization	1.484×10^{-24}
5	GO:BP	GO:0060485	mesenchyme development	4.110×10^{-18}
4	GO:MF	GO:0005201	extracellular matrix structural constituent	8.685×10^{-16}
14	GO:BP	GO:0016055	Wnt signaling pathway	3.688×10^{-15}
6	GO:BP	GO:0030111	regulation of Wnt signaling pathway	1.159×10^{-12}
12	GO:BP	GO:0001935	endothelial cell proliferation	1.621×10^{-10}
7	GO:BP	GO:0035924	cellular response to vascular endothelial growth factor stimulus	9.572×10^{-9}
13	GO:BP	GO:0045766	positive regulation of angiogenesis	9.982×10^{-8}
8	GO:BP	GO:0001837	epithelial to mesenchymal transition	1.452×10^{-7}
10	GO:BP	GO:0032964	collagen biosynthetic process	5.999×10^{-7}
9	GO:BP	GO:0038084	vascular endothelial growth factor signaling pathway	2.946×10^{-6}
11	GO:MF	GO:0017147	Wnt-protein binding	1.515×10^{-3}

Figure 8: RNA Seq analysis of UAS03 treated endothelial cells. SVEC 4-10 cells were treated with Control or 50 μM UAS03, total RNA isolated and RNA Seq performed as described in Methods. (A) Heat map of differentially expressed genes generated using heatmap.2 function gplots package. Genes with q-value <0.05 and FC>1.5 or FC<-1.5 were clustered using hclust function using Pearson's method for genes and Spearman method for samples. (B) Volcano plot of differentially expressed genes created using ggplot. Downregulated genes are represented as blue dots (q<0.05 FC<-1.5) and light blue dots (q<0.05 FC<0 & FC>-1.5).

Upregulated genes represented as red dots (q<0.05 FC>1.5) and gold dots (q<0.05 FC>0 & FC<1.5). Genes highlighted are – top 3 significant differentially expressed genes, top 3 upregulated and downregulated genes with maximum fold change respectively, and genes of interest based on the in-vivo observations with UAS03 treatment. GO term enrichment analysis from the list of significantly upregulated (C) and downregulated (D) genes respectively using gProfiler2. Terms of interest from “Molecular Function” and “Biological Pathway” categories are depicted based on the in-vivo observations with UAS03 treatment. n=3 biological replicates.

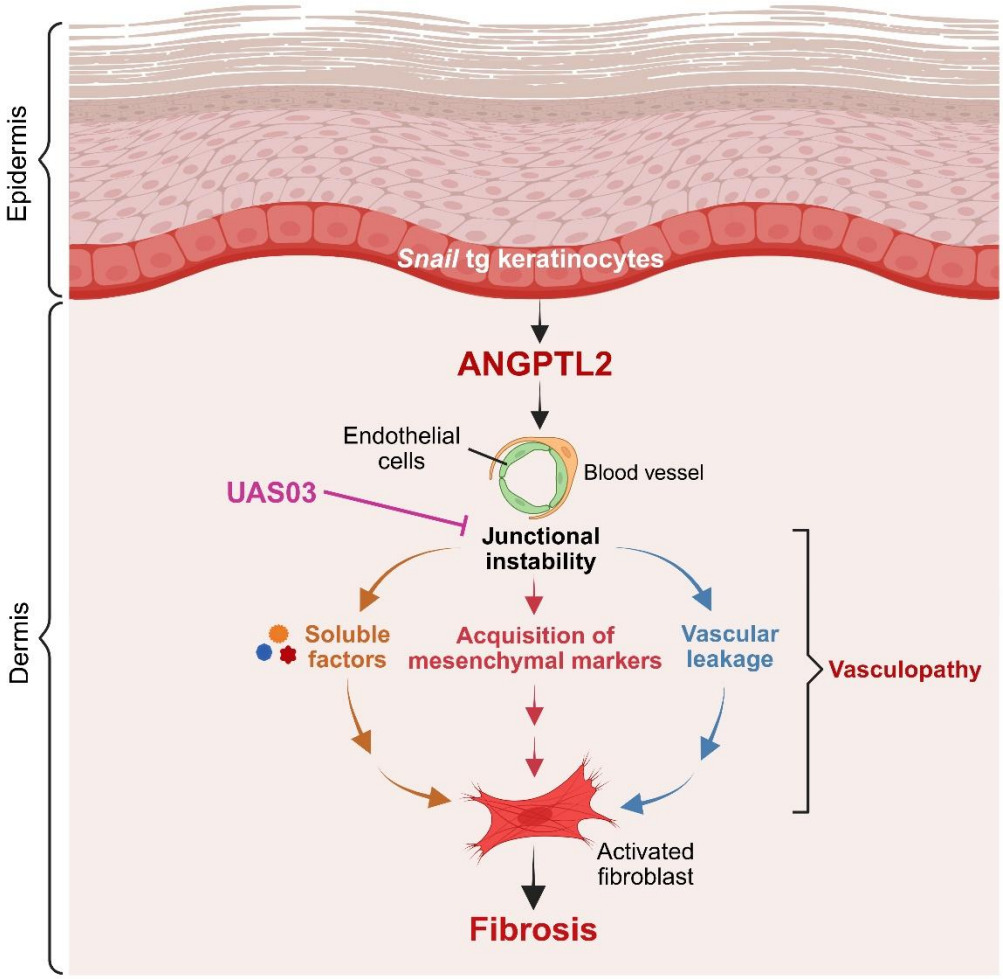

Figure 9: Model demonstrating vasculopathy mediated fibrosis driven by ANGPTL2 in *Snail* tg skin is counteracted by UAS03.

Table 1 – List of quantitative real time PCR primers

Target	Forward primer	Reverse primer
Pdgfb	CATCCGCTCCTTTGATGATCTT	ATGAGCTTTCCAACTCGACTCC
Edn1	CTACGAAGGTTGGAGGCCAT	CGGTTGTGCGTCAACTTCTG
Ctgf	GTGCCAGAACGCACACTG	CCCCGGTTACACTCCAAA
Acta2	ATCGTCCACCGCAAATGC	AAGGAACTGGAGGCGCTG
Angptl2	TCTACTGGGCTGAGTTCCGA	CAGGCAGGGAGAGCTTAGTG
Cldn5	CAAGGTGTATGAATCTGTGCT	GTCAAGGTAACAAAGAGTGCCA
Cdh5	GAACGAGGACAGCAACTTCACC	GTTAGCGTGCTGGTTCCAGTCA
Tjp1	GTTGGTACGGTGCCCTGAAAGA	GCTGACAGGTAGGACAGACGAT
Ocln	TGGCAAGCGATCATACCCAGAG	CTGCCTGAAGTCATCCACACTC
Jam1	CACCTACTCTGGCTTCTCCTCT	TGCCACTGGATGAGAAGGTGAC
Jam3	GCATTGCTTCCAATGACGCAGG	GATGAAGCAGCCTCGTCTGTAC
Fsp1	CAGCACTTCCTCTCTCTTGG	TTTGTGGAAGGTGGACACAA
SM22a	GACATGTTCCAGACTGTTGACCTC	CCTCTTATGCTCCTGGGCTTTCTT
Cnn1	GACGGGATCATTCTTTGCGAA	CCCCATACTTGGTAATGGCTTTG
Tbp	AGTGCCGCCCAAGTAGCA	TCCCCCTCTGCACGTAAATC

Table 2 – SSc patient information

Biopsy Number	Age (years)	Sex	Disease duration	Modified Rodnan Skin Score	Disease classification
1	45	Female	23	10	Diffuse Systemic sclerosis
2	33	Female	5	17	Limited Systemic sclerosis
3	65	Female	15	15	Diffuse Systemic sclerosis
4	50	Female	3	0	Sine Systemic sclerosis
5	23	Female	6	36	Diffuse Systemic sclerosis

Control skin samples were collected from healthy humans with similar age and sex.